iScience

Article

Augmenting flexibility: mutual inhibition between inhibitory neurons expands functional diversity

Graphical abstract

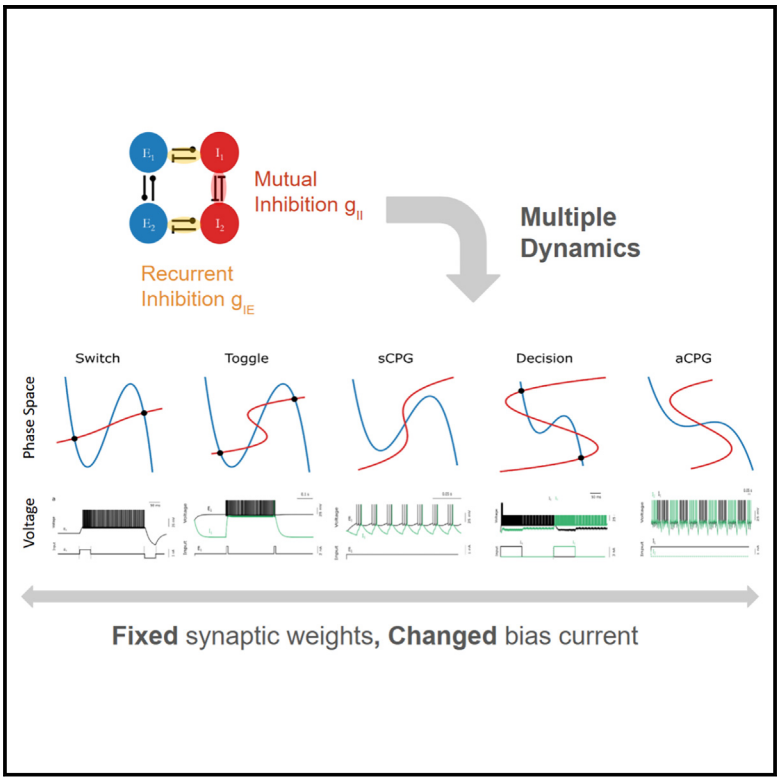

Authors

Belle Liu, Alexander James White, Chung-Chuan Lo

Correspondence

ajw@lolab-nthu.org (A.J.W.), cclo@mx.nthu.edu.tw (C.-C.L.)

In brief

Neuroscience; Theory of computation

Highlights

- Mutual inhibition adds basins of attraction to neural circuits
- Seamless transitions between functions in circuits with coupled mutually connected loops
- Stronger mutual inhibition boosts information storage in large networks

Liu et al., 2025, iScience *28*, 111718
February 21, 2025
https://doi.org/10.1016/j.isci.2024.111718

CellPress

iScience

CellPress
OPEN ACCESS

Article

Augmenting flexibility: mutual inhibition between inhibitory neurons expands functional diversity

Belle Liu,[1,2,5] Alexander James White,[1,3,5,*] and Chung-Chuan Lo[1,4,6,*]
[1]Institute of Systems Neuroscience, National Tsing Hua University, Hsinchu City 30080, Taiwan
[2]Department of Physics, National Tsing Hua University, Hsinchu City 30080, Taiwan
[3]International Intercollegiate Ph.D. Program, National Tsing Hua University, Hsinchu City 30080, Taiwan
[4]Brain Research Center, National Tsing Hua University, Hsinchu City 30080, Taiwan
[5]These authors contributed equally
[6]Lead contact
*Correspondence: ajw@lolab-nthu.org (A.J.W.), cclo@mx.nthu.edu.tw (C.-C.L.)
https://doi.org/10.1016/j.isci.2024.111718

SUMMARY

Recent advances in microcircuit analysis of nervous systems have revealed a plethora of mutual connections between inhibitory interneurons across many different species and brain regions. The abundance of these mutual connections has not been fully explained. Strikingly, we show that neural circuits with mutually inhibitory connections are able to rapidly and flexibly switch between distinct functions. That is, multiple functions coexist for a single set of synaptic weights. Here, we develop a theoretical framework to explain how inhibitory recurrent circuits give rise to this flexibility and show that mutual inhibition doubles the number of cusp bifurcations in small neural circuits. As a concrete example, we study a class of functional motifs we call coupled recurrent inhibitory and recurrent excitatory loops (CRIRELs). These CRIRELs have the advantage of being both multi-functional and controllable, performing a plethora of functions, including decisions, memory, toggle, and so forth. Finally, we demonstrate how mutual inhibition maximizes storage capacity for larger networks.

INTRODUCTION

There are two interesting threads of inquiry when considering recurrent neural networks in a biological context. The first is the preponderance of connections between inhibitory interneurons in real brain networks.[1–6] These mutual connections are found across species from mammals[4,5] to simple organisms such as flies[6] all the way to humans.[1] The second thread hints at the reason that these neural connections are found so ubiquitously, that is, recurrent networks are more flexible.[7–15] All organisms need this flexibly to rapidly respond to their environment, and this is best accomplished by having a single network perform multiple functions[7–11,16–21] without needing to rely on synaptic plasticity to change between functions.[7,12,17–22] This rapid flexibility has been well studied from a dynamic system's perspective[7,12,17,23] and from a biological perspective.[3,13,14,16,17,22,24,25]

It has been hypothesized that a key component of this flexibility is the recurrent nature of neural connections.[12,14,23,26] Often, the focus of recurrent structures is on mutual excitation[8,15,27–30] or feedback inhibition,[5,8,28,31–36] and the role of mutual inhibition tends to receive less attention (the term "recurrent" has been used interchangeably across literature – see Figure 1A for how it is defined in this study). Past computational studies often focus on slower mutual inhibitions role in central pattern generation.[37–39] However, recent advances in multicellular recordings[32,40–43] and simulation studies,[14,41] has given rise to new evidence that suggests that faster mutual inhibition between inhibitory interneuron plays a more crucial role than previously thought.

First, it has been widely reported that inhibitory neurons increase the variability of a network,[5,14,16,44–47] and supporting evidence from connectome studies revealed that mutual inhibition is abundant and formed locally,[6,40,43,44] possibly performing local computations.[5] Second, evidence shows that there are functional differences between feedback and mutual inhibition. For example, feedback inhibition is composed of an interconnected pair of excitatory and inhibitory neurons, which balances the network,[35,36,48] allowing it to approximate an arbitrary motor sequence[12] and are useful in gain control. On the other hand, recurrent inhibition (either feedback or mutual inhibition) increases the number of basins of attraction,[8,39] allowing the network to perform functions such as winner-take-all decision,[8,39,49–51] bistable perception,[41,42] oscillations,[23,26,37,52,53] associative memory[14,54] and grid formation.[53,55] Strikingly, we show a wide variety of these computations can be performed by introducing mutual inhibition into any network. As we will show, that networks with mutual inhibition are able to rapidly

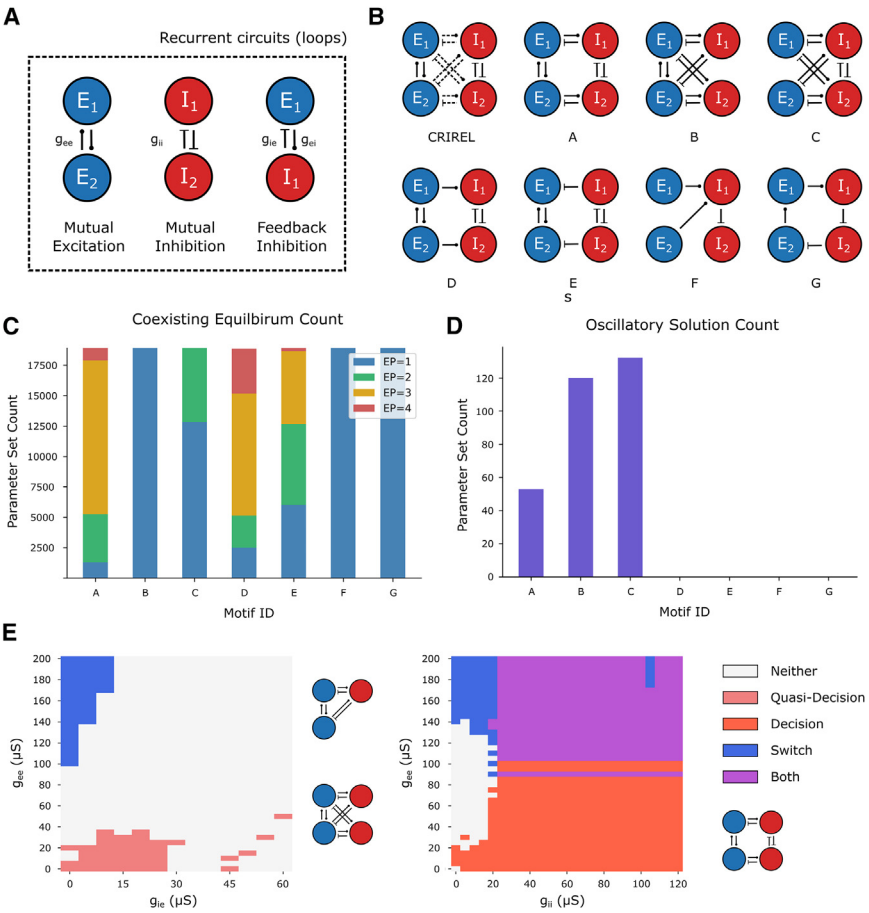

Figure 1. Motifs and statistical analysis of dynamical diversity

(A) Definition of the terms "recurrent" circuits, "mutual" excitation/inhibition and "feedback" inhibition used in this article. Synaptic weights used in part of the results are assigned based on its pre- and post-synaptic neurons, hence there are four types of weights: excitatory-to-excitatory (g_{ee}), excitatory-to-inhibitory (g_{ei}), inhibitory-to-inhibitory (g_{ii}) and inhibitory-to-excitatory (g_{ie}).

(B) The motif labeled "CRIREL" is the definition of CRIREL circuits. The rest of the motifs are indexed by alphabets in no particular order. Blue represents excitation neurons and red inhibition.

(C) Parameter sweep for equilibrium points in different motifs across some parameter space. In this graph, 1 equilibrium point is in blue (EP = 1), 2 is green (EP = 2), 3 is yellow (EP = 3) and 4 is green (EP = 4).

(D) Parameter sweep for CPGs in different motifs across some parameter space.

(E) Parameter sweep for motifs A and B. For motif B (left), the relevant parameters concerning quasi-decision making and switch are g_{ee} and g_{ie}. For motif A (right), the relevant parameters are g_{ee} and g_{ii}. Blue represents regions where the circuit can perform switching, coral-red represents quasi-decision making, red represents decision-making, and white represents no functions present. The purple region is the regime in which the system can perform both functions simultaneously.

switch between multiple functions without changing the synaptic weights. This result, along with supporting connectome studies, all point to the idea that mutual inhibition is crucial in expanding a network's functional repertoire.

At last, we note that a network's functional capacity is not determined solely by the number of synapses.[26,44,48,56] In particular, while each type of synapse increases the number of potential computations a network can have, the network is not necessarily flexible if it cannot seamlessly transition between different functional modes by modulating the parameters. Whether the network is capable of easy transitions is highly dependent on the underlying bifurcation, which is the phenomenon of switching between behavioral characteristics through the change of model parameters.[26,57–59] Specifically, networks near complicated bifurcations are computationally useful,[26] because only networks near a bifurcation have non-trivial dynamics.[12,26,59] In short, one can quickly and precisely control the neural circuit operations by controlling the nearby bifurcation.

Given the lack of attention to mutual inhibition, we set out to systematically model its effect on a network's functionality and dynamics. We hypothesize that mutual inhibition can increase the flexibility of a network by increasing the number of bifurcations the network is near. In particular, it can introduce new functions while subsuming the functions originally present in the network. To further illustrate this argument, we investigated the dynamics of a family of recurrent circuits we dubbed CRIREL (Coupled Recurrent Inhibition and Recurrent Excitation Loop). This type of structure is used across literature regarding a myriad of phenomena, such as decision-making and deviance detection,[4,60] yet the dynamics of this structure require further systematic studies.

To showcase the effect of different recurrent structures on a circuit's dynamics, we first conducted a series of statistical analyses. Based on these statistical results, we then delve into a detailed dynamical analysis of the CRIREL circuit. Our analysis shows how, by including mutual inhibition, even a small 4-neuron circuit is capable of rapidly and flexibly switching between a wide range of computations. Finally, we extend our study to a large random network and show that mutual inhibition is critical for increasing the entropy of its working memory state, implying that mutual inhibition diversifies the dynamical landscape of networks.

RESULTS

Effects of recurrent structures on the complexity of circuit dynamics

We compared several circuit architectures to investigate how different recurrent structures contribute to a circuit's dynamics (Figures 1A and 1B). The first metric we employed to characterize the diversity of circuit behavior was the number of equilibrium points, that is, steady states in firing rate. If the circuit contains multiple equilibrium points, it is more likely to lead to

complex activity patterns in response to different inputs, an indication of the circuit's computational ability.

We begin with the CRIREL circuit, which contains all three recurrent structures, then remove these connections one at a time. Motif A contains all the recurrent structures contained in the other motifs (Figure 1A). Motif B does not contain mutual inhibition, and motif C does not have mutual excitation. In motifs D and E, the feedback inhibition loop is broken – in motif D, feedback inhibition is removed, and in motif E, feedback excitation is removed. Motif F is a pure feedforward structure that was chosen as arbitrarily, and motif G is a feedforward structure that forms a single loop.

For one given motif, we performed a parameter sweep over different synaptic weights and bias currents, totaling up to 18900 parameter settings. Each setting is simulated once, where random perturbations are applied to the neurons to encourage the stochastic exploration of the phase space throughout the trial. Given sufficient intervals between the perturbations, stable equilibrium points should emerge as "clusters" in the firing rate trajectory of the neurons. Therefore, we clustered the entire trajectory using k-means, and the number of clusters within that parameter setting is determined via the elbow method (see STAR Methods for detailed criteria).

The results show that motif A has the largest parameter regime in which the system is not monostable, i.e., the number of equilibrium points exceeds 1 (Figure 1C; monostable in blue). Furthermore, motifs that have mutual inhibition (motifs A, D, E) have parameter sets with equilibrium point counts larger than two, while those with either only mutual excitation or only mutual inhibition have at most counts of two, and feedforward motifs have no bistability at all. In contrast, the presence or absence of feedback inhibition does not make such a large difference in the total number of states possible (albeit feedback can change the parameter regimes these states can be found in). Thus, one can conclude that the combination of mutual excitation and mutual inhibition is the main driver of the multi-state parameter regime but not feedback between the two mutually connected subnetworks.

While the first metric shows the number of equilibrium points in the network, it does not reveal whether other stable structures are possible within the network, such as oscillation given constant input. Therefore, the second metric we employed tested whether central pattern generators (CPG) are present in the network. We count the number of distinct inter-spike intervals (ISI) within the inhibitory neurons, and if the number of ISIs is greater than 1, that implies that there is a CPG (see STAR Methods for more details). This analysis shows that CPGs are only found in A, B, and C – the ones that contain feedback inhibition (Figure 1D).

In summary, we illustrated the functional differences between mutual and feedback inhibition – mutual inhibition increases the number of equilibrium points in the network, while feedback inhibition allows the network to oscillate when given constant input.

Functional differences between feedback and mutual inhibition

The statistical results indicate that mutual inhibition increases the dynamical states, but does not explain the mechanism behind it. Hence, here we consider an explicit example that compares feedback inhibition with mutual inhibition, and compare motif A with motif B. Specifically, we compared the two motifs' ability to perform different functions within some relevant parameter regime.

Motif B contains mutual excitation, which allows it to perform a switch-like function, where some brief positive current pulse can transfer the system to the ON state, and a negative pulse can turn it off. Motif B also has feedback inhibition, which skews the basin of attraction one way, therefore making one of the excitatory neurons fire faster than the other, performing a quasi-decision like function. However, these two functions cannot coexist within the circuit (Figure 1E, left panel). If we add recurrent inhibition to the circuit, however, this problem can be resolved. Consider motif A, which has mutual excitation, feedback inhibition, as well as mutual inhibition. This gives a large parameter regime in which motif A contains both functions simultaneously (Figure 1E, right panel). Here, we stress that even though motif A has more synapses, it is motif B (with mutual inhibition) that is more functional. Therefore, the presence of mutual inhibition can add more functions to the underlying neural network.

Dynamics of coupled recurrent inhibitory and recurrent excitatory loops circuits

All the statistical analyses above point to mutual inhibition is crucial in expanding the functional repertoire of a network. As such, we will focus on Motif A (i.e., CRIREL) and mutual inhibitions effects on coexisting computations. However, to have a better grasp on the functions CRIREL circuits actually bring about, we must look into its dynamics. To this end, we reduced the 4-dimensional CRIREL circuit into a 2-dimensional reduced model, with each of the recurrent circuits compressed into 1 dimension.

$$\tau\frac{dE}{dt} = k_e^* - a_eE + E^3 - \epsilon a_{ie}I \qquad \text{(Equation 1)}$$

$$\tau\frac{dI}{dt} = k_i^* - a_iI - I^3 - \epsilon a_{ei}E \qquad \text{(Equation 2)}$$

Here, a_e, a_i, k_e^*, and k_i^* represent the parameters associated with the cusp bifurcations, while ϵa_{ie} and ϵa_{ei} denote the coupling strengths between the subsystems. A detailed derivation of the reduced model can be found in the Supplementary Note.

Without loss over generality, one can consider a de-dimensionalized form:

$$\tau\frac{dE}{dt} = a_1 - a_2E + E^3 - I \qquad \text{(Equation 3)}$$

$$\tau\frac{dI}{dt} = b_1 - b_2I - I^3 - E \qquad \text{(Equation 4)}$$

Conceptually, it can be understood as preserving the dimensions that are important to the dynamics of interest by considering the properties of the two mutual connections. Here, a_1 and b_1 correspond to the baseline activity level, while a_2 and b_2 roughly represent the mutual excitation and mutual inhibition respectively.

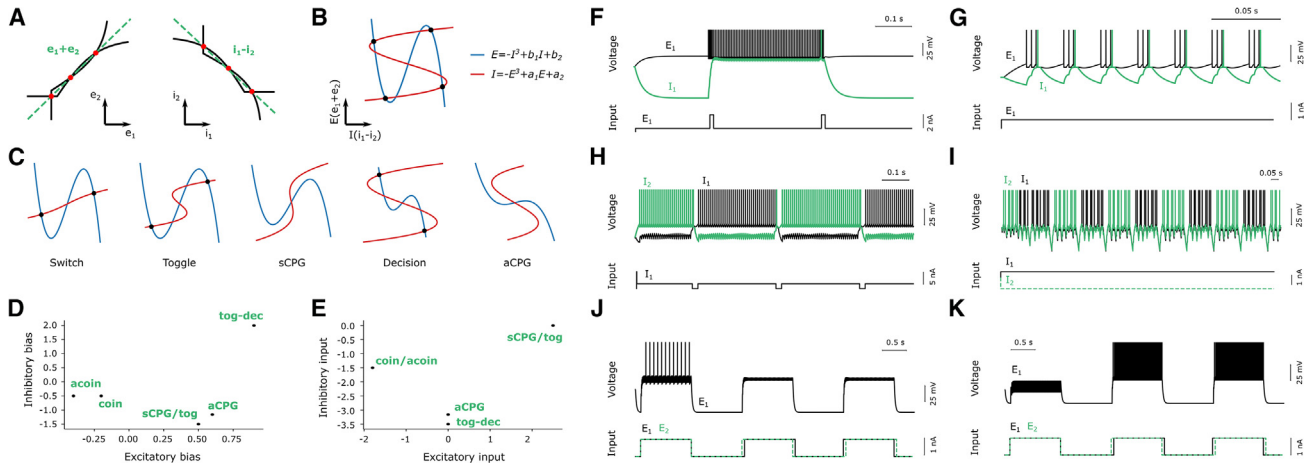

Figure 2. The reduced model of the CRIREL circuit

(A) The phase diagrams of the mutual excitation (left) and inhibition loop (right) when decoupled from one another. The black curves are nullclines and the spots represent equilibrium points. The green dashed line shows the direction in which interesting dynamics lie on (it is only approximate for the inhibitory case).

(B) When weakly coupled together, the CRIREL circuit can be reduced to two dimensions. The blue curve is the nullcline of the mutual excitation loop, the red is the nullcline of mutual inhibition, and the black dots are stable equilibria.

(C) By adjusting the four parameters a_1, a_2, b_1 and b_2, the reduced model will change into different configurations, each of them corresponding to different functions. Demonstration of rapid flexibility using bias currents. All functions coexist for a single set of synaptic weights, namely $g_{ee} = g_{ii} = g_{ei} = g_{ie} = 70\ mS$.

(D) The plot of excitatory and inhibitory bias currents. Each Dot shows the location in bias current parameter space for each function.

(E) The plot of input magnitude excitatory and inhibitory for each function.

(F) Demonstration of the toggle function using square pulses into the excitatory subsystem.

(G) Demonstration of the synchronized CPG function. Note that there is no input, only bias current.

(H) Demonstration of the toggle-decide function using pulses into the inhibitory subsystem.

(I) Demonstration of the anti-synchronized CPG, which again has no input into the network.

(J) Coincidence detection with input into both excitatory and inhibitory subsystems.

(K) Anti-coincidence detection using input into both subsystems.

The simplest spiking neuron one can consider is a leaky integrate-and-fire (LIF) neuron, a neuron that integrates inputs and spikes when it reaches a threshold(see Table 1 for paramters used in this study). LIF neurons act a class 1 excitable neuron,[57] we can approximate each neuron's firing rate as a Wilson-Cowen[26,61] type firing rate model, with each neuron's firing rate as e_1, e_2, i_1 and i_2. This form assumes a monotonic non-linearity. Since mutual excitation tends to synchronize, the dimension of $e_1 - e_2$ is less important than $e_1 + e_2$ if the coupling is much weaker than the mutual connection strength, where e_i represents the firing rate of the excitatory neuron i, which is denoted as E_i. On the other hand, mutual inhibition desynchronizes, therefore $i_1 + i_2$ is less important than $i_1 - i_2$ when the coupling is weak. Similarly, i_j represents the firing rate of inhibitory neuron j, which is denoted as I_j. Hence, by retaining the dimensions of $e_1 + e_2$ and $i_1 - i_2$ only, we can gain a geometrical understanding of how the system operates, which in turn sheds light on the potential computations recurrent circuits can perform (Figure 2A).

The resulting reduced model (Figure 2B) can be visualized using the coordinates $\mathbf{E} \approx e_1 + e_2$ and $\mathbf{I} \approx i_1 - i_2$. The blue and red lines represent the nullclines of **E** and, **I** respectively. Note that both nullclines are of a cubic form, which is the normal form of a cusp bifurcation, thereby proving that mutual connections do indeed add cusp bifurcations to the circuit. Since there are two cubic functions, we know that this system has a double-cusp bifurcation. There are four free parameters in this reduced model, which come from complicated nonlinear mappings of the original neuronal and bias current parameters. For physical intuition, a_1 and b_1 are nonlinear mappings of structural parameters of the neurons, such as capacitance, time constant, or synaptic weights. a_2 and b_2 are mappings from the bias currents into the circuit. These parameters allow the cubic functions to change shape as well as translation, which gives rise to many different phase diagrams (Figure 2C). These phase diagrams correspond to different ''modes'' of the circuit, in which it performs different functions. We will go over all of the functions we discovered later in discussion, but note that this is by no means a complete list of what the circuit is capable of doing.

Rapid flexibility using bias currents to control functionality

Next, we consider a network flexible if multiple functions coexist for a given set of synaptic weights. We are able to reproduce all functions listed in (Figures 2D and 2E) with a single network with a single set of synaptic weights. For demonstration purposes, we chose the synaptic weights $g_{ee} = g_{ii} = g_{ei} = g_{ii} = 70\ mS$.

Strikingly, we are able to use bias current alone to switch between various functions (Figure 2C). Importantly, this endows our network with a set of 6 unique functions (Figures 2F–2J) that can easily and flexibly switched between by modulating bias current and input type. The six functions are toggling (Figure 2F), synchronized CPG (Figure 2G), toggle-decide (Figure 2H),

anti-synchronized CPG (Figure 2I), coincidence detection (Figure 2J), and anti-coincidence detection (Figure 2K).

A nice consequence of this rapid flexibility is to change the functionality on a timescale corresponding to the membrane time constant (here 20 *msec*). It is worth stressing that this does not require a slower change in synaptic weight and that every function is easily accessible from the other functions.

The functions of CRIREL circuits include rudimentary ones that rely more heavily on mutual excitation, such as switch, toggle, and synchronized CPG; it also includes ones in which computations are mainly performed in the mutual inhibition loop, such as decision-making and anti-synchronized CPG. Building from these concepts, we can also have computationally interesting functions, such as working memory, threshold-based filtering, and timing-based decision-making.

Computations in the excitatory subsystem

Switch

We first demonstrate one of the simplest computations, which is a switch-like function (Figure 3A). An intuitive understanding of switching and its behavior is already described in previous sections. Here we demonstrate how to comprehend this function geometrically using the reduced model. The reduced model for the switch has only two stable equilibrium points separated by a saddle equilibrium (Figure 3B). The simulation begins at the equilibrium point where all the neurons are silent, i.e., the OFF state. When a brief positive current pulse is given to one or both of the excitatory neurons, the **E**-nullcline shifts upwards, annihilating the OFF state. Therefore, the system transits to the remaining equilibrium point, i.e., the ON state, and remains there even as the input is removed and the **E**-nullcline returns to its original position. This means that the circuit will continue firing even in the absence of input. When a negative current pulse is applied, the opposite happens, and the system returns to the OFF state. This shows that the circuit is bistable. We see that the reduced model is consistent with the intuitive explanation given above (Figure 3B). Moreover, we tested that this switch into the upstate was present for a broad range of potential input stimuli (Figure 3C).

Computations in the excitatory subsystem with feedback inhibition

Toggle

A function that is similar to a switch is toggle, except that it can be turned off by a positive current pulse instead of a negative pulse. We can visualize this by plotting the voltage traces of one of the excitatory neurons (which are synchronized) and one of the inhibitory neurons (Figure 3D). The first pulse causes the system to go to the ON state, and the firing rate of the inhibitory neurons is insufficient to inhibit the excitatory loop. However, when a second identical pulse enters the system, the firing rate of the excitatory loop increases, and concurrently the inhibitory loop. This extra push is enough for the inhibitory neurons to turn off the excitatory neurons, thus returning the whole system to inactivity.

Again, we can gain insight by examining the phase portrait of the system. The simple shifting mechanism of the switch system no longer applies here. As the impulse current excites the excitatory loop and consequently the inhibition loop, the inhibitory response deepens, causing the inhibitory nullcline to change its shape (Figure 3E). This in turn causes both the ON and OFF states to annihilate, and the system goes from 5 equilibrium points to one unstable spiral node. This means that for a brief amount of time, there exists a limit cycle and the system's state rotates. When the impulse input ends, the inhibitory system relaxes and the 5 equilibrium points return, but by that time the system is already trapped in the ON state. The second pulse repeats the process and rotates the system yet again, allowing it to return to the OFF state. We also examine the required amplitude and duration of stimuli required to toggle the system (Figure 3F). Interestingly, for very long duration the system may rotate a full rotation, rather than a half rotation. This will cause the system not to toggle for long duration stimuli.

Synchronized central pattern generator

The presence of a toggle implies that the circuit is also capable of sustaining periodic oscillations, that is, capable of becoming CPGs. Note that if the impulse current is changed into a constant bias current, the system will repeat the process of toggling over and over again, thus undergoing a synchronized bursting behavior (Figure 3G). The phase diagram of synchronous CPG is the limit-cycle mode (Figure 3H). Moreover, we showed that inhibitory bias current can tune the network over a wide operating frequency (Figure 3I).

Computations in the inhibitory subsystem

Decision making

Switch, toggle and synchronous CPG rely heavily on the dynamics of the mutual excitation loop. Decision-making, on the other hand, is mainly due to mutual inhibition. For a decision network, when two inputs are injected into the neurons E_1 and E_2, the larger of the two inputs will "choose" their corresponding inhibitory neuron, thus preventing the other inhibitory neuron from firing (Figure 4A). Logically, this is the exact counterpart of the switch system, the difference being that the nonlinearity now lies in the **I**-nullcline instead of the **E**-nullcline. While inputs shift the **E**-nullcline either up or down in the switch or toggle phase diagram, it shifts the inhibitory neuron either left or right in this case, hence forcing the system to decide between the two equilibrium points. Geometrically, this corresponds to "rotating" the nullclines of the synchronized CPG by 90° (Figure 4B). To quantify the performance of decision-making, we examined the accuracy and reaction time of the circuit (Figure 4C). The results are consistent with decision-making networks containing two competing populations of excitatory neurons – as the input becomes more coherent, accuracy increases and reaction time decreases.

Anti-toggle (anti-synchronized toggle)

Just as decision-making is the counterpart of the switch function, anti-toggle is the counterpart of toggle. By taking advantage of the reduced model, we can rotate the nullclines by 90° to generate an anti-toggle from toggle. This is achieved by swapping the parameters of the excitatory and inhibitory systems. As with the case of toggling, in this mode, the excitatory neurons of the excitatory sub-circuit can be turned on and off by positive input pulses. The difference is that now when one inhibitory neuron is turned off, the other one automatically turns on

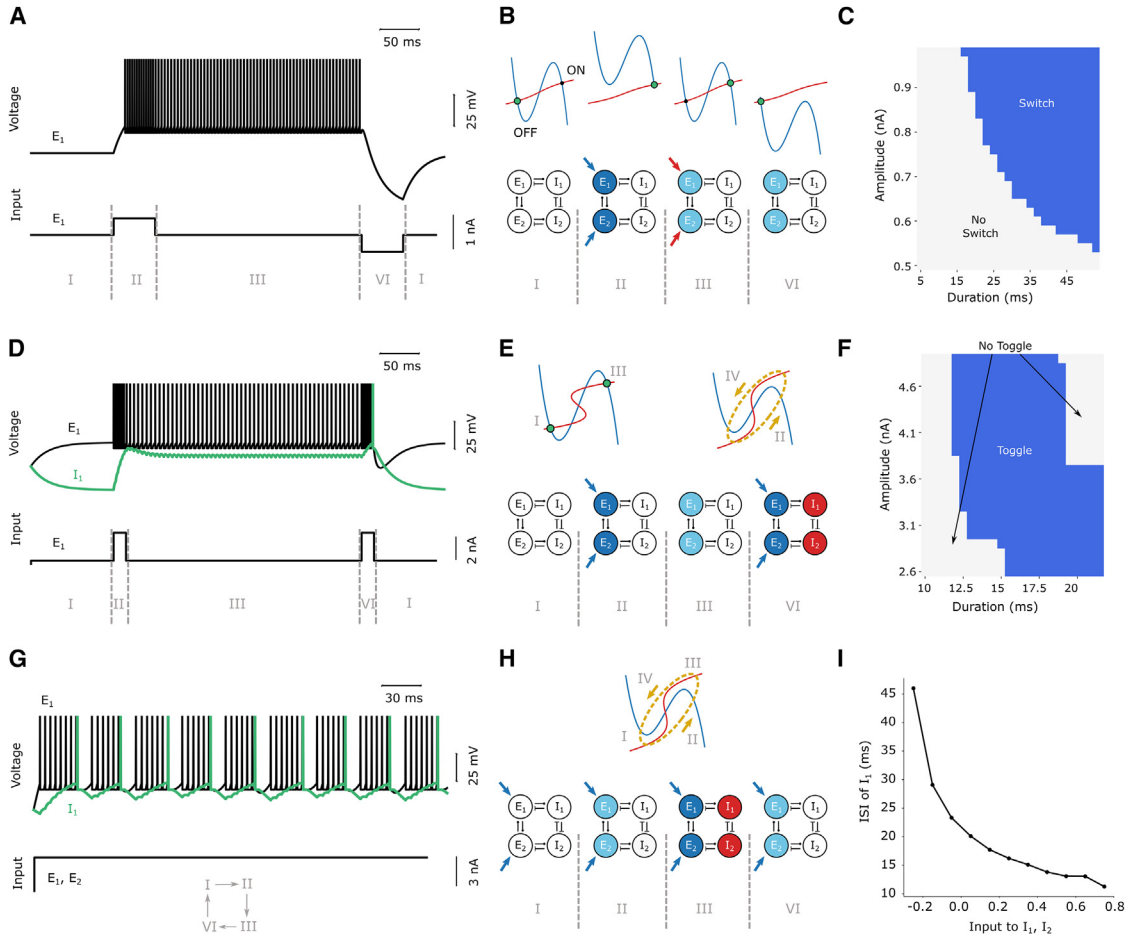

Figure 3. Switch, toggle, and synchronous CPG

(A) Switch voltage traces. Top row: the voltage trace of neuron E_1. Bottom row: the current input into E_1. The Roman numerals represent different phases of the input and correspond to the Roman numerals shown in panel (b).

(B) Switch phase diagrams and schematics of neural activity. Top row: switch function phase diagram. The green dot represents the state of the system. Bottom row: Schematic diagram of the relative activity of each neuron during different time periods. Blue represents excitation and red inhibition. The darker the color, the higher the activity.

(C) Inputs that induce a switch. A parameter sweep over the duration and amplitude of the input pulse that induces a switch into the upstate. Blue represents stimuli that induce a switch, while gray represents those that do not.

(D) Toggle voltage traces. Top row: the voltage traces of E_1 (in black) and I_1 (in green). Bottom row: the current given to E_1. The Roman numerals correspond to the Roman numerals shown in panel (E).

(E) Toggle phase diagrams and schematics of neural activity. Top row: toggle function phase diagram. Bottom row: Schematic diagram of the firing rates of each neuron during different time periods.

(F) Inputs that induce a toggle. A parameter sweep over the duration and amplitude of the input pulse that toggles between the upstate and downstate. Blue represents stimuli that induce a switch, while gray represents those that do not.

(G) synchronous CPG voltage traces. The rows are identical to those of (D). Here, however, the current into E1 is changed from pulses into a constant input. The Roman numerals arranged in a loop means that the four phases occur repeatedly.

(H) sCPG phase diagrams and schematics of neural activity.

(I) ISI of inhibitory spikes. Parameter sweep over the inhibitory bias current, and its effect on the period of the CPG.

(Figures 4D and 4E). This function is extremely robust, as it works in a wide range of parameters (Figure 4F).

Asynchronized central pattern generator

Similar to how toggle gives rise to synchronized CPGs, we can do the same for anti-toggle to an anti-synchronized CPG. by changing the current pulses into a constant bias. This change will not directly yield anti-synchronized CPGs, since a constant bias would be reinforcing the system to stay within the same equilibrium point. However, if we introduce timescale separation, e.g., mechanisms such as slow GABA synapses, calcium dynamics, and second-messenger systems, the circuit can oscillate. We can visualize this by taking advantage of a limit cycle in the reduced system (Figures 4G and 4H). Again, we examined how the inhibitory bias current controls the operating frequency of the CPG (Figure 4I), and showed that it operates over a wide range of frequencies.

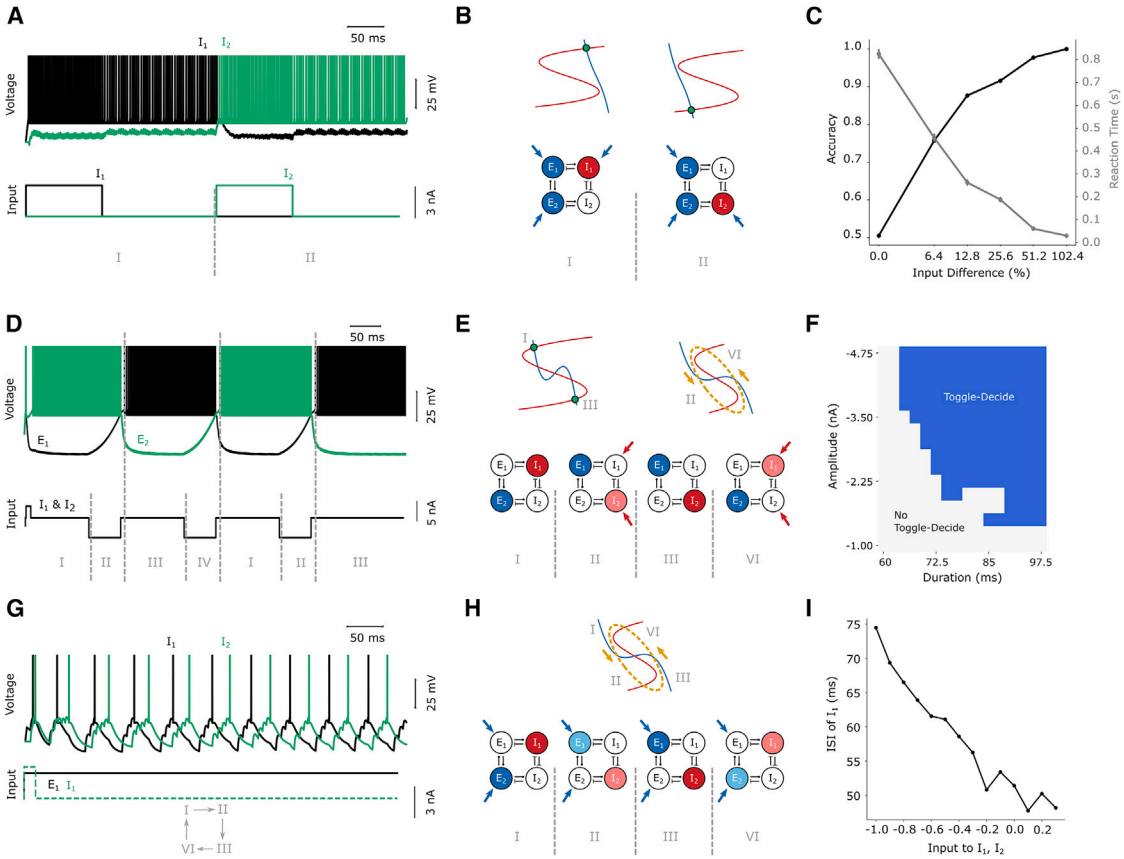

Figure 4. Decision-making and asynchronous CPG

(A) Decision-making voltage traces. Top row: the voltage traces of I_1 (in black) and I_2 (in green). Bottom row: the current given to I_1 (in black) and I_2 (in green). Here, E_1 and E_2 are given constant bias currents to maintain the decision after the input is removed.

(B) Decision-making phase diagrams and schematics of neural activity.

(C) Psychometric function of decision-making. As the input difference between the two inputs increases, the accuracy (black) increases, and the reaction time (gray) decreases. The error bar for the reaction time represents its standard error.

(D) Anti-toggle voltage traces.

(E) Anti-toggle phase diagrams and schematics of neural activity.

(F) A parameter sweep over the duration and amplitude of the input pulse that anti-toggle. Blue represents stimuli that induce an anti-toggle, while gray represents those that do not.

(G) Asynchronous CPG voltage traces.

(H) Asynchronous CPG phase diagrams and schematics of neural activity.

(I) ISI of inhibitory spikes. Parameter sweep over the inhibitory bias current, and its effect on the period of the CPG.

Computations in the coupled recurrent inhibitory and recurrent excitatory loops system

Working memory

The situation described above complicated when the bistability of the excitatory sub-system is combined with the decision-making of the inhibitory sub-system. Since the ON state exists, this means that the decision can be remembered even after the input is withdrawn because of the excitatory sub-system. When receiving strong input, the excitation sub-system enters the ON state asymmetrically. One of the excitatory neurons will have higher firing rates, thus allowing its neighboring inhibitory neuron to fire and inhibit the other one. Furthermore, the feedback inhibition strength is not strong enough to turn the excitatory sub-system off, thus the system "remembers" the input (Figure 5).

There are two protocols to change the memory currently being maintained in the system. One can clear the system with a reset signal and the system will return to rest (Figure 5A). The memory can also be overwritten directly (Figures 5B–5D).

The analysis of this system is identical to the decision-making system, except that there could be 4 equilibrium points (Figure 5E). It can indeed be confirmed that this nullcline configuration is present in the full CRIREL system, where the inhibitory neurons can either be both on (i.e., (1, 1)), one on and one off (i.e., (1, 0) or (0, 1)) or both off (i.e., (0, 0)). Thus, this system is capable of forming a working memory system with 2-bit memory. This is a perfect example of how simple functions such as decision-making and switching can combine to yield more interesting and useful functions.

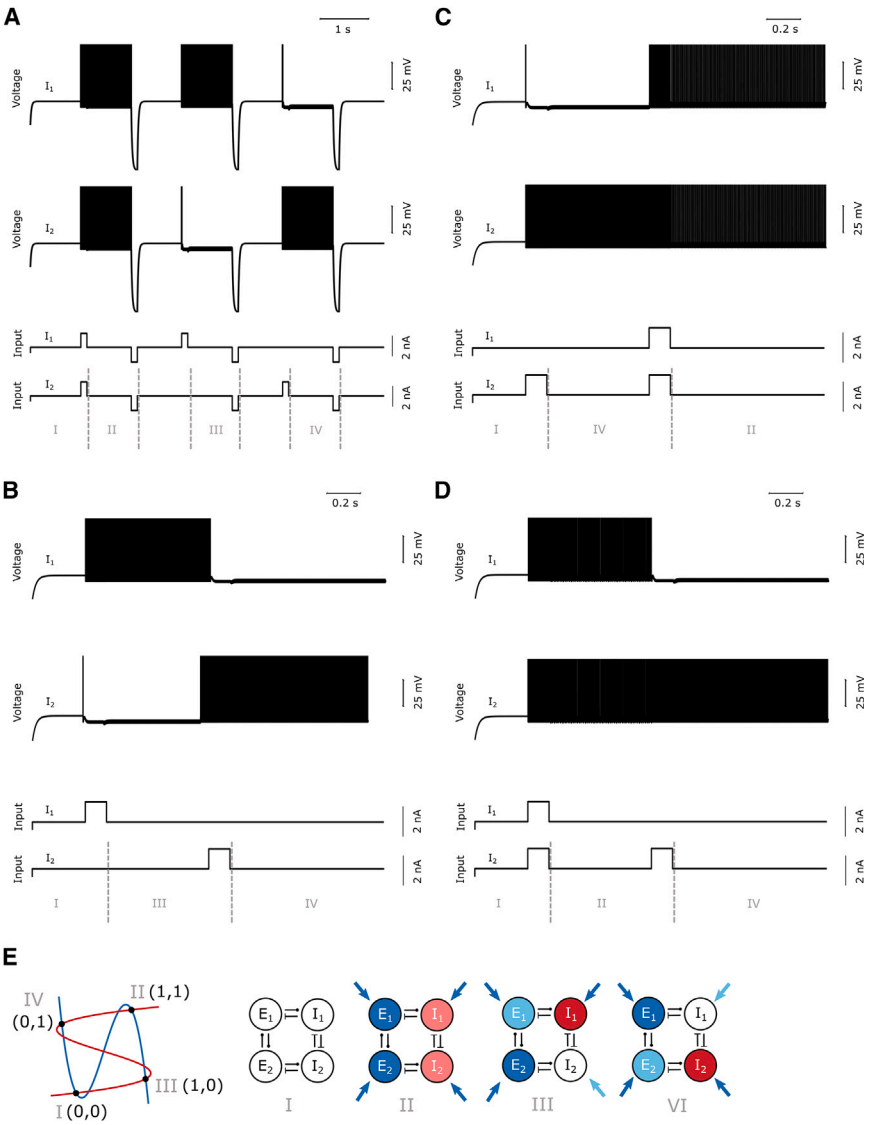

Figure 5. Working memory

(A) Voltage trace. This circuit stores a "two bit" signal in working memory, i.e., (1,1), (1,0), (0,1), and (0,0), corresponding to (I_1 on, I_2 on), (I_1 on, I_2 off), (I_1 off, I_2 on), (I_1 off, I_2 off). This can be seen in the top two rows of the graph, showing the voltage traces of I_1 and I_2. The bottom two rows are the inputs to the four neurons.

(B–D) Switching memory without reset.

(B) Switching from 1,0 to 0,1.

(C) Switching from 0,1 to 1,1.

(D) Switching from 1,1 to 0,1.

(E) Working memory phase diagrams and schematics of neural activity. Top row: phase diagram. Bottom row: Schematic diagram of the neural activity.

Threshold-based filtering

The capability of making decisions allows CRIRELs to be utilized in many different ways, including useful functions such as creating a safety net for hyperactivity. If we allow the CRIREL circuit to take on asymmetrical parameters (Figure 6A, left) of membrane and synapse, the circuit can become a low-pass filter in terms of amplitudes, where small inputs are remembered by the circuit (working memory like), and larger ones terminate the bistability (toggle like) (Figure 6B). This computation is possible precisely due to the presence of asymmetries in the network. When one of the excitatory neurons receives a small input, since I_1 has stronger synaptic weights, I_1 will be chosen and thus inhibit I_2. However, when the input is sufficiently large, I_2 has smaller capacitance and time constants than I_1, and therefore will be excited faster than I_1, thus winning the decision. The feedback inhibition from I_1 is weak, therefore when I_1 is chosen, it does not affect the network's bistability; however, the feedback inhibition from I_2 is strong, therefore whenever I_2 is chosen, the network shuts down. Hence, the circuit serves as a gateway that filters out inputs that are too large, which could be potentially useful for preventing epilepsy. The threshold of the circuit can be adjusted by manipulating the bias current of I_1 (Figure 6C).

Timing-based detection

Aside from making decisions based on the magnitude of the input, what is perhaps even more intriguing is detecting the relative timing of inputs (Figures 6D and 6E). Even a sub-millisecond difference between the inputs is sufficient for the network to perceive. Timing-based detections can be accomplished if we allow sufficiently strong feedback inhibition, as we did in toggling. Under this condition, two modes are allowed: the coincidence detection mode (Figure 6D) and the anti-coincidence detection mode (Figure 6E). In the anti-coincidence mode, the network will choose whichever input came first but will turn off completely if inputs arrive at the same time. In the coincidence mode, the network will only fire if the inputs arrive simultaneously (Figure 6E). Note that for these two modes, an additional neuron is added to the CRIREL circuit that combines the output of E_1 and E_2 (Figure 6A, right). However, this extra neuron is only added for the sake of having a more clear-cut output. The computation for these two modes is still done within the CRIREL circuit itself.

Here, coincidence is controlled primarily by mutual excitation. The synaptic input is sufficient to turn the system on when both inputs arrive at the same time, but if there is a delay in the system, then the system will not fire. Conversely, the anti-coincidence system takes advantage of the toggle like dynamics, where it turns the system off if and only if both inputs arrive simultaneously. Otherwise, the inhibitory neurons do not fire with sufficient strength to turn the system off. Coincidence has a narrow range of operation (Figure 6F) because it relies on a more delicate balance between the inhibitory and excitatory subsystems.

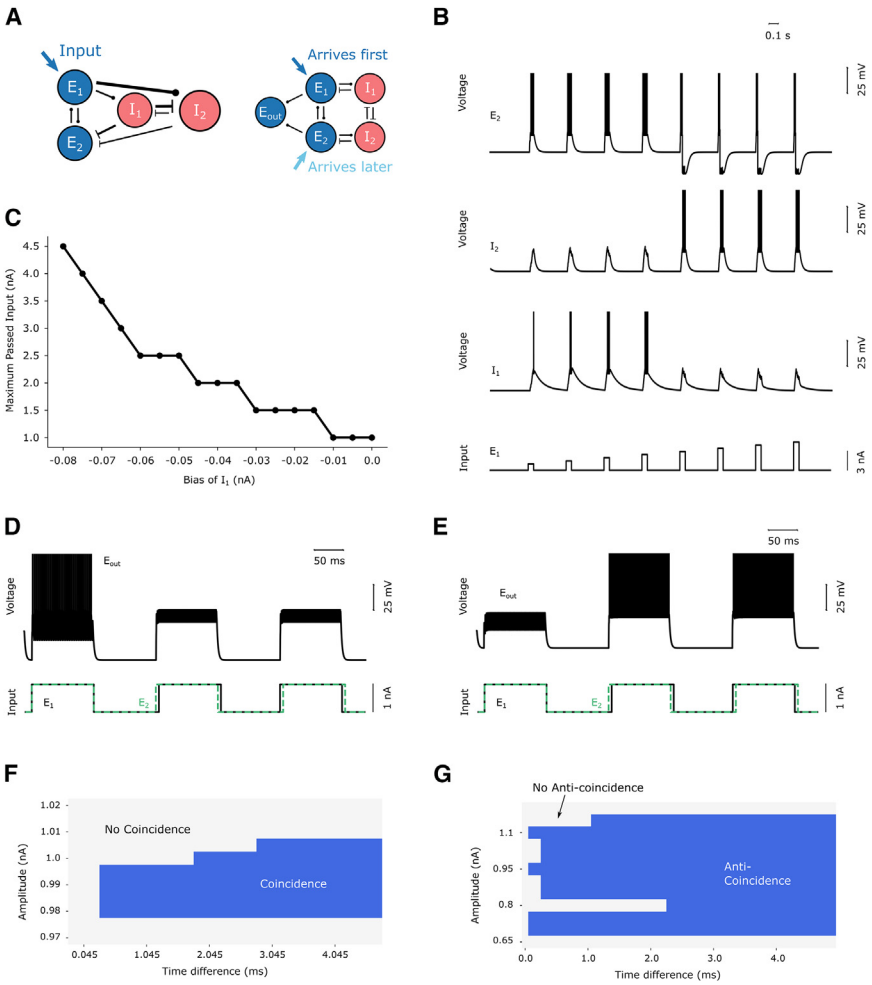

Figure 6. Threshold and timing based decisions

(A) Circuit motifs for threshold-based filtering (left) and timing-based detection (right). The asymmetries of the parameters are shown schematically in the diagram: thicker lines represent larger weights, and vice versa.

(B) Voltage traces of threshold-based filtering. The top three rows show the voltage traces of E_2, I_2, and I_1, and the bottom row shows the injected current into E_1. Here we inject neuron E_1 with different pulses of increasing amplitude.

(C) Maximum amplitude of input that passes the filter as a function of bias into I_1. The steps are discrete because the input we used is discrete.

(D) Timing-based detection, coincidence mode. The top row is the voltage trace for the output neuron. The bottom row is the input for E_2 (in black) and E_1 (in green). Since the timing difference between the input is small (5 ms), for visual demonstration the difference is exaggerated.

(E) Timing based detection, anti-coincidence-mode. The top row is the voltage trace for the output neuron. The bottom row is the input for E_2 (in black) and E_1 (in green). (f-g) A parameter sweep for both coincidence (F) and anti-coincidence (G) over both amplitude of signal and timing difference. Blue represents the existence of the function, while light gray represents its absence.

On the other hand, anti-coincidence operates over a much broader range of parameters (Figure 6G).

Memory in large network

So far, we have explicitly explained how mutual inhibition adds a cusp bifurcation to the circuit, which allows the circuit to perform various functions. Here, we extend this argument to large random networks. We focused on the function of working memory in particular, as working memory requires the use of both on-off switches (excitatory cusps) as well as decision-making (inhibitory cusps). We showed that an increase in mutual inhibition strength allows the network to have a wider variety of memory states. However, other functions that are present in the CRIREL circuit can also be reproduced in the large network as well (see Figure S3).

The random network consists of 100 neurons, 75 excitatory and 25 inhibitory, where each connection has a 50 percent probability of being present (Figure 7A). g_{ie} and g_{ii} are varied from 0 to approximately 30 (μS). For each parameter set, the excitatory neurons of the network are given random current pulses, and after the stimulation stops the network relaxes into a steady state. Since the stimulation is random, each time the steady state might be identical or different, and this is repeated 100 times per parameter set. Each steady state is recorded as a "word," where different words represent different steady states (Figure 7B; see STAR Methods). The entropy for the distribution of the words across 100 trials, H_{word}, is calculated for the various parameter sets, which reflects how diverse the steady states are (Figure 7C).

For the same g_{ie} value, H_{word} increases as g_{ii} increases (Figures 7C and 7D). To understand the reason behind this, we turn to two other entropy measures, H_{symbol} and H_{binary} (Figure 7B). Simply put, H_{symbol} measures how diverse the firing rate across the population is, for a single trial. If the activities of all neurons are high (Figure 7D left) then there are not a lot of symbols available to form a word, hence H_{symbol} would be low and consequentially H_{word} as well. Moreover, It can be shown that there is a regime of suitable g_{ii} to g_{ie} ratio where H_{symbol} is maximized (Figure 7C). This trend is quite different from H_{word}, where it increases almost monotonically with g_{ii}. Therefore, an increase in the number of symbols is not the main mechanism behind what we observed in H_{word}.

Therefore, we used yet another method for calculating entropy, H_{binary}. Here, if a neuron fires, it is labeled as "1," while a silent neuron is labeled "0" (Figure 7B). Each time the network relaxes into a steady state, it yields a distribution of 1s and 0s across the neuron population, and the entropy for that distribution is calculated. Essentially, if the neurons' firing rates are more "all or nothing" (or "winner takes all") – so that the ratio

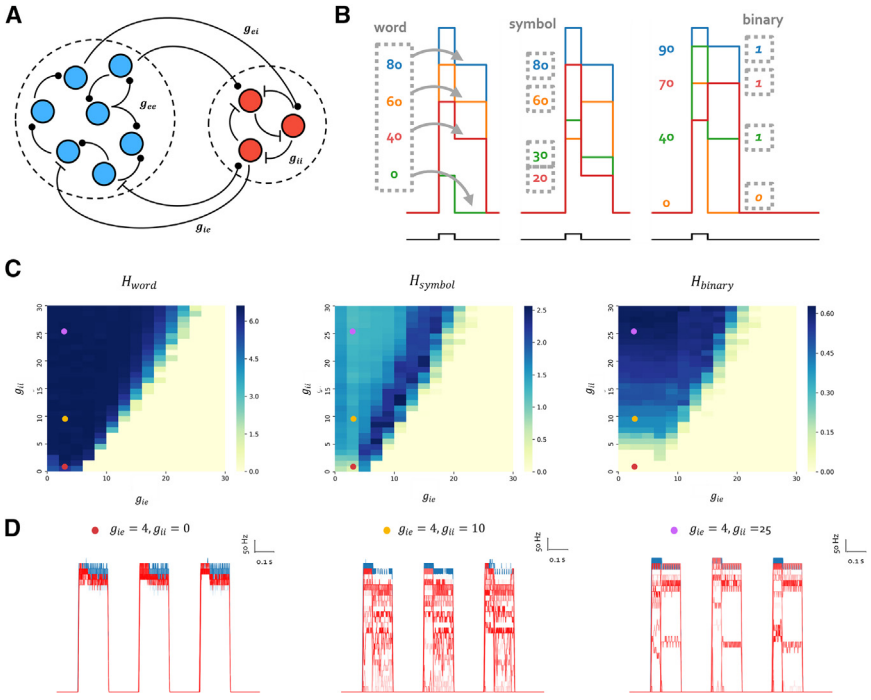

Figure 7. Memory in a large network

(A) Schematic diagram of a large random network.

(B) Schematic diagram of how entropy is calculated. Each line represents the firing rate of a neuron, and the firing rate of the neuron population is defined as a "word." The words across 100 trials form a probability mass function, which is used to calculate H_{word}. The word itself is also a probability mass function for different firing rates, which also has an associated entropy. The trial average of this entropy is called H_{symbol}. Alternatively, each neuron can be labeled as on (1) or off (0), and the entropy associated with this is called H_{binary}.

(C) From left to right: H_{word}, H_{symbol}, H_{binary} for different g_{ii} and g_{ie}.

(D) Firing rate traces for neurons across 3 trials, with different synaptic weights. Each trial showcases how the steady state activity differs between having different g_{ii} values. Blue traces represent excitatory neurons, and red traces inhibitory neurons. From left to right: increasing g_{ii}.

between the count of 1s and 0s is more equal – then H_{binary} will be higher. Moreover, H_{binary} is augmented as g_{ii} increases, which follows a similar trend to H_{word} (Figure 7C), implying that the increase in memory capacity as shown by H_{word} may be caused by the neurons' firing becoming more "all or nothing," which is in turns due to an increase in g_{ii}.

Furthermore, we note that for large g_{ii} values, its entropy value is near maximal. That is, if all 100 trials result in unique states, then $H_{word} = \log_2 \frac{1}{100} \approx 6.64$, and we see that the entropy values of large g_{ii} are near that value.

To conclude, increasing g_{ii} increases the number of memory states the network contains. Consistent with how mutual inhibition introduces new bifurcations to the CRIREL circuit, mutual inhibition in a large network also complicates its dynamics and yields a more computationally useful product. The large network is also capable of performing other functions found in the CRIREL circuit (Figure S3).

DISCUSSION

In the present study, we show that mutual inhibition plays a key role in increasing the computation complexity and functional repertoire. This is evident from: (1) motifs that contain mutual inhibition exhibit more functions than those without, (2) the ability of a specific class of the motif, called CRIREL, to rapidly and flexibly switch between multiple biologically relevant functions for the same set of synaptic weights, and (3) higher working memory capacity in large neural networks with mutual inhibition than those without. We also demonstrate that the key mechanism underlying the functionality of mutual inhibition lies in its ability to increase the basins of attraction from an increase in the underlying cusp bifurcations.

It is not that networks lacking mutual inhibition, especially those with more neurons, cannot perform the tasks described, but rather that mutual inhibition expands the repertoire of the motif. For example, feedback inhibition (motif B) can support oscillatory solutions. However, the double cusp bifurcation present in the CRIREL circuit allows for the coexistence of oscillatory solutions and decision-like computations. Therefore, we focus on the CRIREL motif to examine how it can simultaneously encompass and switch between a diverse range of functions.

Here, we specifically looked at one instantiation of CRIREL to make finding and investigating functions more tractable. It turns out that If a network is composed solely of diagonal connections without straight connections, it essentially behaves as the same circuit, as the network could be untwisted without altering its function. However, in cases where both diagonal and straight connections are present—forming an all-to-all connected network with uniform synaptic weights—the network effectively functions as a single inhibitory neuron. This observation led to a focus on the CRIREL motif as an optimal representation of mutual inhibition. One would surmise that a gradual transition from the investigated structure to a fully connected network by incrementally strengthening the diagonal connections, certain network functions, such as decision-making and anti-synchronized central pattern generators (CPGs), are likely to become more challenging to achieve. Teasing out exactly the dynamics of the diagonal coupling effect on decisions would be fascinating for future work.

This is in line with past research, as connections between inhibitory neurons have been shown in many different contexts.[1,2,5,31,33,34,37,39,43,44] It is interesting to note that in a recent study[6] that reconstructed single-cell level brain-wide connectome of fruit flies,[62–64] putative inhibitory neurons receive more inhibitory than the excitatory inputs. Moreover, studies in the hippocampus of rats have found a plethora of mutually

Table 1. Parameters for neuronal model and synaptic model

Spiking Neural Model Parameters			
Parameter	Value	Parameter	Value
C_m	0.5 (nF)	τ_{AMPA}	2 (ms)
τ	20 (ms)	V_{AMPA}	0 (mV)
E_L	−70 (mV)	τ_{GABA}	5 (ms)
V_{reset}	−55 (mV)	V_{GABA}	−90 (mV)
V_{Th}	−50 (mV)	–	–

inhibitory parvalbumin interneurons.[43] Most Strikingly, the human cortex has a preponderance of inhibitory-to-inhibitory connections compared to the mouse cortex.[1] These findings imply the importance of mutual inhibition in the brain network. We have shown computationally that these types of connections are useful and perform a unique role in computational processing by expanding the number of computational states a network has. We also hypothesize the existence of a function called anti-toggle, that is capable of seamlessly switching between different basins of attraction, which is potentially useful in tracking changes of state, working memory based decisions, or even counting. Furthermore, the existence of decisions and anti-toggle in the inhibitory subnetwork could potentially be one mechanism behind the simultaneous suppression and excitation of inhibitory interneurons observed in various studies of cortical neurons.[4,5,44]

Moreover, our results are in line with studies that have reported an increase in variability[4,44] and working memory maintenance[14] when the connection strength of inhibition is increased. In our study, we showed that increases in g_{ii} are more responsible for the increase in the number of steady states than g_{ie}. This tracks with the presence of a multiple cusp bifurcation. As the large network simulations showed, for each inhibitory neuron with all-to-all inhibitory connections added, there is an additional cusp bifurcation. This doubles the number of unique combinations of states the network can perform.

Other domains of biology are also finding that mutual inhibition (also called repression) is a key player. Recent studies in genetic networks have shown gene networks are topologically organized into groups that can mutually inhibit each other, and give rise to distinct phenotype.[65] Similar mutual inhibitory networks have also been found in the immune system,[66] and cell differentiation networks.[67] These works could suggest a role for mutual inhibition increasing information storage/functionality in domains more general than neural architecture.

One area our research can be extended to is examining the effects of gap junctions on the network. Some have found that mutual inhibition and gap junctions tend to coexist in some circuits.[43] It has been shown that gap junctions have a tendency to average out the winner-take-all aspect of the decisions.[68,69]

A final direction for future work is to examine the best way to control networks with mutual inhibition. Several studies have suggested that networks near bifurcations are computationally useful.[12,26,58,59] Some studies use balanced inhibition to tune the network to be useful.[12] Here, we wonder if this process can be used to control networks with mutual inhibition. If mutual inhibition is removed, are these networks still computationally useful?

To conclude, we have shown that mutual inhibition is key to expanding the functionality of the network. This is possible because mutual inhibition expands the number of cusp bifurcations in a network. Ultimately, this helps elucidate why neural circuits in the brain are so flexible in their operation and are capable of such rich dynamics.

Limitations of the study

In addition, in our study, we have mostly overlooked plastic synapses. Several studies have shown that this is an important component in network functionality.[19,26,52,54,56] Moreover, recent work has shown that synaptic depression can desegregate different cusp bifurcations by weakening the strong synaptic effects between mutual excitatory loops.[48,70] Aside from that, by using plastic synapses, one can construct networks that are both balanced and near bifurcations.[12] In this article, different functions require different synaptic weights. It is possible that a motif circuit can switch between functions based on learning or plasticity-induced weight changes. This can be a future direction of this study.

RESOURCE AVAILABILITY

Lead contact

Requests for further information and resources should be directed to and will be fulfilled by the lead contact, Chung-Chuan Lo (cclo@mx.nthu.edu.tw).

Material availability

This study did not generate new unique reagents.

Data and code availability

- Code: All code used can be found at the github: https://github.com/L24358/CRIREL
- Data: All data can be generated by the code found on the github.
- All other requests: Any additional information required to reanalyze the data reported will be shared by the lead contact upon request.

ACKNOWLEDGMENTS

We thank Gabrielle Gutierrez for discussion and feedback on the figures, Youngmin Park for useful discussions on the mathematical proofs presented in the study, and Fred Rieke and Peter J. Thomas for feedback on the article. This work is partially supported by the Featured Areas Research Center Program within the framework of the Higher Education Sprout Project, a joint fund from the Ministry of Education (MOE) and the Ministry of Science and Technology (MOST) in Taiwan. This work is also partially supported by the National Science and Technology Council (Taiwan) grants 111-2311-B-007-011-MY3, 113-2218-E-007-019- and 113-2321-B-002-029-.

AUTHOR CONTRIBUTIONS

CCL provided supervision for the entire project. BL/AJW discovered the functions and developed the theory. BL/AJW/CCL developed simulations and robustness tests. BL/AJW ran simulations. BL/AJW/CCL wrote the article. All Authors have approved of the article.

DECLARATION OF INTERESTS

The authors declare no competing interests.

STAR★METHODS

Detailed methods are provided in the online version of this paper and include the following:

- KEY RESOURCES TABLE
- METHOD DETAILS
  - Spiking neural model and synaptic model
  - CRIREL function simulations
  - Large random network
  - Dynamical analysis
  - Decoupled mutual excitation and mutual inhibition
  - Coupling mutual excitation with inhibition
- QUANTIFICATION AND STATISTICAL ANALYSIS
  - Equilibrium points in microcircuits
  - Parameter space
  - Clustering
  - CPG in microcircuits
  - Decision-making and bistability
  - Entropy
  - Entropy of words, H_{word}
  - Entropy of symbols, H_{symbol}
  - Entropy of binary symbols, H_{binary}

SUPPLEMENTAL INFORMATION

Supplemental information can be found online at https://doi.org/10.1016/j.isci.2024.111718.

Received: June 5, 2024
Revised: November 6, 2024
Accepted: December 27, 2024
Published: January 1, 2025

REFERENCES

1. Loomba, S., Straehle, J., Gangadharan, V., Heike, N., Khalifa, A., Motta, A., Ju, N., Sievers, M., Gempt, J., Meyer, H.S., and Helmstaedter, M. (2022). Connectomic comparison of mouse and human cortex. Science *377*, eabo0924.
2. Pfeffer, C.K., Xue, M., He, M., Huang, Z.J., and Scanziani, M. (2013). Inhibition of inhibition in visual cortex: the logic of connections between molecularly distinct interneurons. Nat. Neurosci. *16*, 1068–1076.
3. Churchland, M.M., Cunningham, J.P., Kaufman, M.T., Ryu, S.I., and Shenoy, K.V. (2010). Cortical preparatory activity: representation of movement or first cog in a dynamical machine? Neuron *68*, 387–400.
4. Najafi, F., Elsayed, G.F., Cao, R., Pnevmatikakis, E., Latham, P.E., Cunningham, J.P., and Churchland, A.K. (2020). Excitatory and Inhibitory Subnetworks Are Equally Selective during Decision-Making and Emerge Simultaneously during Learning. Neuron *105*, 165–179.e8.
5. Yu, J., Hu, H., Agmon, A., and Svoboda, K. (2019). Recruitment of GABAergic interneurons in the barrel cortex during active tactile behavior. Neuron *104*, 412–427.e4.
6. Huang, Y.-C., Wang, C.-T., Su, T.-S., Kao, K.-W., Lin, Y.-J., Chuang, C.-C., Chiang, A.-S., and Lo, C.-C. (2018). A Single-Cell Level and Connectome-Derived Computational Model of the Drosophila Brain (Frontiers).
7. Yang, G.R., Joglekar, M.R., Song, H.F., Newsome, W.T., and Wang, X.-J. (2019). Task representations in neural networks trained to perform many cognitive tasks. Nat. Neurosci. *22*, 297–306.
8. Wang, X.-J. (2008). Decision Making in Recurrent Neuronal Circuits. Neuron *60*, 215–234.
9. Morton, D.W., and Chiel, H.J. (1994). Neural architectures for adaptive behavior. Trends Neurosci. *17*, 413–420.
10. Leonard, J.L. (2000). Network Architectures and Circuit Function: Testing Alternative Hypotheses in Multifunctional Networks. Brain Behav. Evol. *55*, 248–255.
11. Marder, E., and Thirumalai, V. (2002). Cellular, synaptic and network effects of neuromodulation. Neural Network. *15*, 479–493.
12. Hennequin, G., Vogels, T.P., and Gerstner, W. (2014). Optimal Control of Transient Dynamics in Balanced Networks Supports Generation of Complex Movements. Neuron *82*, 1394–1406.
13. Shew, W.L., Yang, H., Yu, S., Roy, R., and Plenz, D. (2011). Information Capacity and Transmission Are Maximized in Balanced Cortical Networks with Neuronal Avalanches. J. Neurosci. *31*, 55–63.
14. Kim, R., and Sejnowski, T.J. (2021). Strong inhibitory signaling underlies stable temporal dynamics and working memory in spiking neural networks. Nat. Neurosci. *24*, 129–139.
15. Douglas, R.J., Koch, C., Mahowald, M., Martin, K.A., and Suarez, H.H. (1995). Recurrent excitation in neocortical circuits. Science *269*, 981–985.
16. Machens, C.K., Romo, R., and Brody, C.D. (2005). Flexible Control of Mutual Inhibition: A Neural Model of Two-Interval Discrimination. Science *307*, 1121–1124.
17. Lyttle, D.N., Gill, J.P., Shaw, K.M., Thomas, P.J., and Chiel, H.J. (2017). Robustness, flexibility, and sensitivity in a multifunctional motor control model. Biol. Cybern. *111*, 25–47.
18. Shenoy, K.V., Kaufman, M.T., Sahani, M., and Churchland, M.M. (2011). A dynamical systems view of motor preparation: Implications for neural prosthetic system design. Prog. Brain Res. *192*, 33–58.
19. Destexhe, A., and Marder, E. (2004). Plasticity in single neuron and circuit computations. Nature *431*, 789–795.
20. Harris-Warrick, R., and Marder, E. (1991). Modulation of neural networks for behavior. Annu. Rev. Neurosci. *14*, 39–57.
21. Bargmann, C.I. (2012). Beyond the connectome: how neuromodulators shape neural circuits. Bioessays *34*, 458–465.
22. Marder, E., and Taylor, A.L. (2011). Multiple models to capture the variability in biological neurons and networks. Nat. Neurosci. *14*, 133–138.
23. Beer, R.D. (1995). On the Dynamics of Small Continuous-Time Recurrent Neural Networks. Adapt. Behav. *3*, 469–509.
24. Webster-Wood, V.A., Gill, J.P., Thomas, P.J., and Chiel, H.J. (2020). Control for multifunctionality: bioinspired control based on feeding in Aplysia californica. Biol. Cybern. *114*, 557–588.
25. Neustadter, D.M., Herman, R.L., Drushel, R.F., Chestek, D.W., and Chiel, H.J. (2007). The kinematics of multifunctionality: comparisons of biting and swallowing in Aplysia californica. J. Exp. Biol. *210*, 238–260.
26. Hoppensteadt, F.C., and Izhikevich, E.M. (1997). Weakly Connected Neural Networks. In Applied Mathematical Sciences (Springer-Verlag).
27. Litwin-Kumar, A., and Doiron, B. (2012). Slow dynamics and high variability in balanced cortical networks with clustered connections. Nat. Neurosci. *15*, 1498–1505.
28. Peng, Y., Barreda Tomás, F.J., Klisch, C., Vida, I., and Geiger, J.R.P. (2017). Layer-specific organization of local excitatory and inhibitory synaptic connectivity in the rat presubiculum. Cerebr. Cortex *27*, 2435–2452.
29. Seeman, S.C., Campagnola, L., Davoudian, P.A., Hoggarth, A., Hage, T.A., Bosma-Moody, A., Baker, C.A., Lee, J.H., Mihalas, S., Teeter, C., et al. (2018). Sparse recurrent excitatory connectivity in the microcircuit of the adult mouse and human cortex. Elife *7*, e37349.
30. Holmgren, C., Harkany, T., Svennenfors, B., and Zilberter, Y. (2003). Pyramidal cell communication within local networks in layer 2/3 of rat neocortex. J. Physiol. *551*, 139–153.
31. Wang, X.-J. (2010). Neurophysiological and computational principles of cortical rhythms in cognition. Physiol. Rev. *90*, 1195–1268.
32. Isaacson, J.S., and Scanziani, M. (2011). How inhibition shapes cortical activity. Neuron *72*, 231–243.
33. Durstewitz, D., Seamans, J.K., and Sejnowski, T.J. (2000). Neurocomputational models of working memory. Nat. Neurosci. *3*, 1184–1191.

34. Ferguson, K.A., and Cardin, J.A. (2020). Mechanisms underlying gain modulation in the cortex. Nat. Rev. Neurosci. *21*, 80–92.
35. Herstel, L.J., and Wierenga, C.J. (2021). Network control through coordinated inhibition. Curr. Opin. Neurobiol. *67*, 34–41.
36. Sadeh, S., and Clopath, C. (2021). Inhibitory stabilization and cortical computation. Nat. Rev. Neurosci. *22*, 21–37.
37. Whittington, M.A., Traub, R.D., Kopell, N., Ermentrout, B., and Buhl, E.H. (2000). Inhibition-based rhythms: experimental and mathematical observations on network dynamics. Int. J. Psychophysiol. *38*, 315–336.
38. Ermentrout, B. (1992). Complex dynamics in winner-take-all neural nets with slow inhibition. Neural Network. *5*, 415–431.
39. Van Vreeswijk, C., Abbott, L.F., and Bard Ermentrout, G. (1994). When inhibition not excitation synchronizes neural firing. J. Comput. Neurosci. *1*, 313–321.
40. Pelkey, K.A., Chittajallu, R., Craig, M.T., Tricoire, L., Wester, J.C., and McBain, C.J. (2017). Hippocampal gabaergic inhibitory interneurons. Physiol. Rev. *97*, 1619–1747.
41. Kogo, N., Kern, F.B., Nowotny, T., Ee, R.v., Wezel, R.v., and Aihara, T. (2021). Dynamics of a mutual inhibition between pyramidal neurons compared to human perceptual competition. J. Neurosci. *41*, 1251–1264.
42. Koyama, M., and Pujala, A. (2018). Mutual inhibition of lateral inhibition: a network motif for an elementary computation in the brain. Curr. Opin. Neurobiol. *49*, 69–74.
43. Espinoza, C., Guzman, S.J., Zhang, X., and Jonas, P. (2018). Parvalbumin + interneurons obey unique connectivity rules and establish a powerful lateral-inhibition microcircuit in dentate gyrus. Nat. Commun. *9*, 4605.
44. Haroush, N., and Marom, S. (2019). Inhibition increases response variability and reduces stimulus discrimination in random networks of cortical neurons. Sci. Rep. *9*, 4969.
45. Buzsáki, G., and Wang, X.-J. (2012). Mechanisms of Gamma Oscillations. Annu. Rev. Neurosci. *35*, 203–225.
46. Ben-Ari, Y. (2002). Excitatory actions of gaba during development: the nature of the nurture. Nat. Rev. Neurosci. *3*, 728–739.
47. Feller, M.B. (1999). Spontaneous Correlated Activity in Developing Neural Circuits. Neuron *22*, 653–656.
48. Mongillo, G., Rumpel, S., and Loewenstein, Y. (2018). Inhibitory connectivity defines the realm of excitatory plasticity. Nat. Neurosci. *21*, 1463–1470.
49. Wang, C.-T., Lee, C.-T., Wang, X.-J., and Lo, C.-C. (2013). Top-down modulation on perceptual decision with balanced inhibition through feedforward and feedback inhibitory neurons. PLoS One *8*, e62379.
50. Lo, C.-C., and Wang, X.-J. (2006). Cortico–basal ganglia circuit mechanism for a decision threshold in reaction time tasks. Nat. Neurosci. *9*, 956–963.
51. Wong, K.-F., and Wang, X.-J. (2006). A Recurrent Network Mechanism of Time Integration in Perceptual Decisions. J. Neurosci. *26*, 1314–1328.
52. Marder, E., Goeritz, M.L., and Otopalik, A.G. (2015). Robust circuit rhythms in small circuits arise from variable circuit components and mechanisms. Curr. Opin. Neurobiol. *31*, 156–163.
53. Ermentrout, B. (1998). Neural networks as spatio-temporal pattern-forming systems. Rep. Prog. Phys. *61*, 353–430.
54. Hopfield, J.J. (1982). Neural networks and physical systems with emergent collective computational abilities. Proc. Natl. Acad. Sci. USA *79*, 2554–2558.
55. Couey, J.J., Witoelar, A., Zhang, S.-J., Zheng, K., Ye, J., Dunn, B., Czajkowski, R., Moser, M.-B., Moser, E.I., Roudi, Y., and Witter, M.P. (2013). Recurrent inhibitory circuitry as a mechanism for grid formation. Nat. Neurosci. *16*, 318–324.
56. Chen, B., and Miller, P. (2020). Attractor-state itinerancy in neural circuits with synaptic depression. J. Math. Neurosci. *10*, 15.
57. Izhikevich, E.M. (2007). Dynamical Systems in Neuroscience (MIT Press).
58. Buendía, V., di Santo, S., Villegas, P., Burioni, R., and Muñoz, M.A. (2020). Self-organized bistability and its possible relevance for brain dynamics. Phys. Rev. Res. *2*, 013318.
59. Toups, J.V., Fellous, J.-M., Thomas, P.J., Sejnowski, T.J., and Tiesinga, P.H. (2012). Multiple Spike Time Patterns Occur at Bifurcation Points of Membrane Potential Dynamics. PLoS Comput. Biol. *8*, e1002615.
60. Chien, V.S.C., Maess, B., and Knösche, T.R. (2019). A generic deviance detection principle for cortical On/Off responses, omission response, and mismatch negativity. Biol. Cybern. *113*, 475–494.
61. Wilson, H.R., and Cowan, J.D. (1973). A mathematical theory of the functional dynamics of cortical and thalamic nervous tissue. Kybernetik *13*, 55–80.
62. Shih, C.-T., Sporns, O., Yuan, S.-L., Su, T.-S., Lin, Y.-J., Chuang, C.-C., Wang, T.-Y., Lo, C.-C., Greenspan, R.J., and Chiang, A.-S. (2015). Connectomics-based analysis of information flow in the Drosophila brain. Curr. Biol. *25*, 1249–1258.
63. Shih, C.-T., Lin, Y.-J., Wang, C.-T., Wang, T.-Y., Chen, C.-C., Su, T.-S., Lo, C.-C., and Chiang, A.-S. (2020). Diverse Community Structures in the Neuronal-Level Connectome of the Drosophila Brain. Neuroinformatics *18*, 267–281.
64. Chiang, A.-S., Lin, C.-Y., Chuang, C.-C., Chang, H.-M., Hsieh, C.-H., Yeh, C.-W., Shih, C.-T., Wu, J.-J., Wang, G.-T., Chen, Y.-C., et al. (2011). Three-Dimensional Reconstruction of Brain-wide Wiring Networks in Drosophila at Single-Cell Resolution. Curr. Biol. *21*, 1–11.
65. Hari, K., Ullanat, V., Balasubramanian, A., Gopalan, A., and Jolly, M.K. (2022). Landscape of epithelial–mesenchymal plasticity as an emergent property of coordinated teams in regulatory networks. Elife *11*, e76535.
66. Misawa, T., SoRelle, J.A., Choi, J.H., Yue, T., Wang, K.-w., McAlpine, W., Wang, J., Liu, A., Tabeta, K., Turer, E.E., et al. (2020). Mutual inhibition between prkd2 and bcl6 controls t follicular helper cell differentiation. Sci. Immunol. *5*, eaaz0085.
67. Duddu, A.S., Sahoo, S., Hati, S., Jhunjhunwala, S., and Jolly, M.K. (2020). Multi-stability in cellular differentiation enabled by a network of three mutually repressing master regulators. J. R. Soc. Interface *17*, 20200631.
68. Lau, T., Gage, G.J., Berke, J.D., and Zochowski, M. (2010). Local dynamics of gap-junction-coupled interneuron networks. Phys. Biol. *7*, 16015.
69. Kopell, N., and Ermentrout, B. (2004). Chemical and electrical synapses perform complementary roles in the synchronization of interneuronal networks. Proc. Natl. Acad. Sci. USA *101*, 15482–15487.
70. Miller, P., Brody, C.D., Romo, R., and Wang, X.-J. (2003). A recurrent network model of somatosensory parametric working memory in the prefrontal cortex. Cerebr. Cortex *13*, 1208–1218.
71. Syakur, M.A., Khotimah, B.K., Rochman, E.M.S., and Satoto, B.D. (2018). Integration K-Means Clustering Method and Elbow Method For Identification of The Best Customer Profile Cluster. IOP Conf. Ser. Mater. Sci. Eng. *336*, 012017.

STAR★METHODS

KEY RESOURCES TABLE

REAGENT or RESOURCE	SOURCE	IDENTIFIER
Software and algorithms		
FlySim	Y.C. Huang et al. 2018	https://doi.org/10.3389/fninf.2018.00099
Mathematica	Wolfram	Wolfram.com&SoftwareforPloting
Code	–	https://github.com/L24358/CRIREL

METHOD DETAILS

Spiking neural model and synaptic model

All simulations in this study are run on flysim.[6] Each individual neuron was modeled as a leaky integrate-and-fire neuron:

$$C_m\frac{dV}{dt} = -\frac{C_m}{\tau}(V - E_L) + \sum I_{j,r}^{syn}(t) \quad \text{(Equation 5)}$$

$$\text{When } V > V_{Th} \text{ then } V \to V_{reset}, t \to t + t_{reset} \quad \text{(Equation 6)}$$

where C_m is the capacitance, V the membrane potential, τ is the time constant, E_L the reversal potential, and I_j^{syn} the current from the j^{th} presynaptic neuron, and r represents the receptor. When the membrane potential reaches V_{Th}, the neuron fires, and is promptly reset to V_{reset} after an amount of time t_{reset}. The parameters can be found in Table 1.

Excitation is modeled as an exponentially decaying AMPA receptor, while inhibition is modeled as an exponentially decaying GABA receptor. More precisely, we have excitatory and inhibitory currents given by

$$I_r(t) = g_r s_r(t)(V - E_r)$$

$$\tau_r\frac{ds_r}{dt} = -s + \sum_{t_{spike}}\delta(t_{spike} - t)$$

Here, r represents the receptor $(r \in \{AMPA, GABA\})$, I is the current of the receptor, V is the membrane potential, E is the reverse potential, g is the conductance of the receptor, s is the gating variable for the receptor ion channel. s is governed by a linear ODE with time constant τ, and is forced by a sum of Dirac delta impulses $\sum_{t_{spike}}\delta(t_{spike} - t)$, where t_{spike} is the timing of presynaptic spikes. It is important to note that $g_{ee} = g_{AMPA}$ when both pre and post synaptic neurons are excitatory and $g_{ei} = g_{AMPA}$ when the presynaptic neuron is excitatory and postsynaptic neuron is inhibitory. Likewise, $g_{ii} = g_{GABA}$ when both pre and post synaptic neurons are inhibitory and $g_{ie} = g_{GABA}$ when the presynaptic neuron is inhibitory and postsynaptic neuron is excitatory.

CRIREL function simulations

The reduced model allowed us to predict the different functions the CRIREL circuit may be capable of performing. These functions are actualized by simulation. While the reduced model is general for the whole class of CRIREL circuits, the results we have shown are simulated on one particular circuit (motif A in Figure 1B), with the exception of threshold-based filtering, which is simulated on motif H (Figure 6A). The parameters for simulation are listed in Table S3, and the stimulation is shown in the results section. Parameter searches are illustrated in detail below.

Switch, toggle and anti-toggle

The robustness of the functions determines how realistically they can be implemented in noisy biological systems. For switch, toggle and anti-toggle, we swept through appropriate regimes to showcase its working parameter range (Figures 3C, 3F, and 4F). A pulse of a specific amplitude and duration was given to the circuit, in the same manner as displayed in Figures 3A and 3D and Figure 4F, respectively.

If the circuit is turned on – defined as the mean firing rate larger than zero in the designated time period (200-400 ms) – and off – defined as the mean firing rate equal to zero after 500 ms, then the circuit is deemed capable of performing switch/toggle within said parameter set. Toggling is furthermore sensitive to the precise timing of the second pulse near the transition to toggling functionality, which means that within certain parameter sets, the behavior of toggling is not robust when the onset or offset pulse timing varies. Therefore, the onset of the pulse is varied from 500-505 ms, and the circuit is only labeled as capable of performing toggling if it toggles for all 6 onset times.

Similarly, a parameter set is defined as performing anti-toggle if the designated neuron fires after the duration of the input ends, and the other gradually returns to silence (evaluated by seeing if the designated neuron has a higher firing rate than the other).

sCPG and aCPG

For central pattern generators, the ability to adjust their firing period is essential (Figures 3I and 4I). This can be achieved by modifying its input into the inhibitory neurons. Again, the protocol mimics those of Figures 3G and 4G respectively. The ISI of the inhibitory neurons is calculated by averaging all the ISIs within one simulation trial, while disregarding the initial ISI.

Decision-making

The psychometric function of the decision-making circuit is shown to quantify its accuracy and reaction time (Figure 4C). The input difference 2*c* (%) is defined similarly to those of,[8] where the input to one population (in our case, one inhibitory neuron) is $1 + c$, and the input for the other neuron is $1 - c$, and c ranges from 0 to 1. Essentially, the larger the input difference, the easier the decision is to make. The input lasts for 100 ms. The accuracy is defined as the number of correct trials over total trials, and in cases where no decision is reached, the winning population is randomly assigned. The reaction time is defined as the time from which the stimulus begins to the time when one population reaches the threshold firing rate of 200 Hz. In cases with no decisions, the reaction time is set at 2s. The mean reaction time is then calculated by averaging over all 500 trials.

Threshold-based filtering

By tuning the bias current of I_1, the threshold of the filter can be adjusted. The stimulation used here is identical to those of Figure 6B. The input "passes" the threshold when the maximum firing rate of E_2 reaches 100 Hz within 100 ms after stimulation. Note that the maximum passed input amplitude appears to be discrete because the input used in Figure 6B is discrete itself.

Coincidence and anti-coincidence detectors

Similar to how we tested the working parameter range for switch and toggle, we swept through different pulse amplitudes and timing differences for the coincidence and anti-coincidence detectors. A working parameter set is defined as the circuit firing according to its truth table (1 for the firing rate larger than zero, and 0 for the firing rate equal to zero).

Large random network

To determine whether the flexibility of mutual inhibition is preserved in larger networks, we built a larger network and investigated a specific function, memory. To construct the large network, we used 100 LIF neurons with the same membrane parameters as the microcircuits. The excitatory population had 75 neurons, while the inhibitory population had 25 neurons. The parameters for connection probability and synaptic weights are given in Table S4.

Each excitatory neuron was given a random 500 ms pulse with an amplitude drawn from a normal distribution with mean $\mu = 3$ and variance, $\sigma^2 = 3$ in addition to an underlying bias current of -5 nA. After the pulse ended, we waited for an extra 1 s before giving a reset signal of -20 nA to the excitatory neurons. Through this protocol, if the network is capable of sustaining memory, then it will settle into a random equilibrium point after the positive pulse is removed, and before the reset signal arrives. Three different types of entropy are calculated to analyze the variety of memory states in the network.

Dynamical analysis

A reduced model was used to gain a deeper understanding of the dynamics of the CRIREL circuit. Here we derive the reduced model that we use to organize our results. The reduced model allows us to conceptually understand what is occurring dynamically in the spiking neural network. Furthermore, the intuition gained from the reduced model is invaluable, as any function found in the reduced model can also be found in the spiking model for an appropriate set of parameters. This is a consequence of central manifold reduction. Note that this does *not* work in the converse direction, meaning there could be functions in the spiking model that are not in the reduced model.

For further understanding of the statistical results, we reduced the CRIREL system into a two-dimensional model given by the equations

$$\tau \frac{dE}{dt} = k_e^* - a_e E + E^3 - \epsilon a_{ie} I \qquad \text{(Equation 7)}$$

$$\tau \frac{dI}{dt} = k_i^* - a_i I - I^3 - \epsilon a_{ei} E \qquad \text{(Equation 8)}$$

where, a_e, a_i, k_e^*, and k_i^* are the parameters of the cusp bifurcations. ϵa_{ie} and ϵa_{ie} are the coupling strengths between each subsystem. The full derivation of the reduced model is given in the Supplementary Note. In this paper we only consider small ϵ, and consider large ϵ out of the scope of this paper. The reduced model allows us to conceptually understand what is occurring dynamically in the spiking neural network. Furthermore, the intuition gained from the reduced model is invaluable, as any function found in the reduced model can also be found in the spiking model for an appropriate set of parameters. Note that this does *not* work in the converse direction, meaning there could be functions in the spiking model that are not in the reduced model. This is especially apparent when ϵ is not small.

As a broad overview, we first begin by showing that the mutual excitatory loop and the mutual inhibitory loop each have a cusp bifurcation. Then we prove that feedback inhibition cannot undergo a cusp bifurcation. Next, we show that when coupled together, both cusps are maintained. Then finally, we work out the reduced model's simple cubic form.

Decoupled mutual excitation and mutual inhibition

We begin with a simple firing-rate model for the mutual excitation loop:

$$\tau \frac{de_1}{dt} = -e_1 + f(b + g_{ee}e_2) \quad \text{(Equation 9)}$$

$$\tau \frac{de_2}{dt} = -e_2 + f(b + g_{ee}e_1) \quad \text{(Equation 10)}$$

and mutual inhibition:

$$\tau \frac{di_1}{dt} = -i_1 + f(b - g_{ii}i_2) \quad \text{(Equation 11)}$$

$$\tau \frac{di_2}{dt} = -i_2 + f(b - g_{ii}i_1) \quad \text{(Equation 12)}$$

Here, e_1, e_2, i_1, and i_2 are the firing rates of the neurons, and τ is a time constant. Our two bifurcation parameters are the bias current b and the synaptic weight g_{ee} or g_{ii}, depending on the type of mutual connection. Because the LIF spiking model we use is a class 1 excitable neuron[57] (it has a continuous input frequency curve), we assume that $f(x)$ is monotonic, i.e., $f'(x) \geq 0$.

To begin, we need to find the cusp bifurcation point. A necessary condition of the bifurcation point is the point at which one of the eigenvalues of the Jacobian is 0. Thus we calculate the Jacobians for our system at the equilibrium point (denoted with a * superscript) and find:

$$J_e = \frac{1}{\tau}\begin{pmatrix} -1 & g_{ee}f'\left(b + g_{ee}e_2^*\right) \\ g_{ee}f'\left(b + g_{ee}e_1^*\right) & -1 \end{pmatrix} \quad \text{(Equation 13)}$$

and for inhibition:

$$J_i = \frac{1}{\tau}\begin{pmatrix} -1 & -g_{ii}f'\left(b - g_{ii}i_2^*\right) \\ -g_{ii}f'\left(b - g_{ii}i_1^*\right) & -1 \end{pmatrix} \quad \text{(Equation 14)}$$

Note here that f' is positive. Simplifying the notation and letting $f'_{x_k} = f'(b \pm g_{xx}x_k^*)$

$$\det(J_e) = \frac{1}{\tau}\det\begin{pmatrix} -1 & g_{ee}f'_{e_2} \\ g_{ee}f'_{e_1} & -1 \end{pmatrix} = \frac{1}{\tau}\left(1 - g_{ee}^2 f'_{e_1} f'_{e_2}\right) = 0 \quad \text{(Equation 15)}$$

$$\det(J_i) = \frac{1}{\tau}\det\begin{pmatrix} -1 & -g_{ii}f'_{i_2} \\ -g_{ii}f'_{i_1} & -1 \end{pmatrix} = \frac{1}{\tau}\left(1 - g_{ii}^2 f'_{i_1} f'_{i_2}\right) = 0 \quad \text{(Equation 16)}$$

Thus there will be at least a saddle node bifurcation whenever $g_{ee} = \sqrt{\frac{1}{f'_{e_1} f'_{e_2}}}$ or $g_{ii} = \sqrt{\frac{1}{f'_{i_1} f'_{i_2}}}$.

Note that for feedback inhibition we cannot even have a saddle-node bifurcation. If we examine the firing-rate model

$$\tau \frac{de_1}{dt} = -e_1 + f(b - g_{ii}i_1) \quad \text{(Equation 17)}$$

$$\tau \frac{di_1}{dt} = -i_1 + f(b + g_{ee}e_1) \quad \text{(Equation 18)}$$

we see that the Jacobi can never have a 0 eigenvalue.

$$\det(J_{ei}) = \frac{1}{\tau}\det\begin{pmatrix} -1 & -g_{ie}f'_{i_1} \\ g_{ei}f'_{e_1} & -1 \end{pmatrix} = \frac{1}{\tau}\left(1 + g_{ei}g_{ie}f'_{e_1} f'_{i_1}\right) > 0 \quad \text{(Equation 19)}$$

This is because all terms are restricted to be positive. Thus feedback inhibition can only have one stable fixed point.

The next step here to prove that we have a cusp bifurcation, and not just a saddle-node bifurcation, is to prove that the quadratic part of the system degenerates. To do this we need to find a center manifold, expand along that manifold, and show that the quadratic term can be zero. We begin by finding the center manifold for the two systems. This is a one-dimensional surface such that $e_2 = M_e(e_1)$ and $i_2 = M_i(i_1)$.

We can calculate the manifold by noting that

$$\frac{de_2}{dt} = \frac{dM_e(e_1)}{dt} = \frac{dM_e}{de_1}\frac{de_1}{dt}. \quad \text{(Equation 20)}$$

and

$$\frac{di_2}{dt} = \frac{dM_i(i_1)}{dt} = \frac{dM_i}{di_1}\frac{di_1}{dt}. \quad \text{(Equation 21)}$$

Solving for M_i and M_e gives us

$$\frac{dM_e}{de_1} = \frac{-M_e(e_1)+f(b+g_{ee}e_1)}{-e_1+f(b+g_{ee}M_e(e_1))} \quad \text{(Equation 22)}$$

$$\frac{dM_i}{di_1} = \frac{-M_i(i_1)+f(b-g_{ii}i_1)}{-i_1+f(b-g_{ii}M_i(i_1))} \quad \text{(Equation 23)}$$

In this particular case the excitatory manifold is easier to algebraically determine the excitatory manifold, so we will proceed only with the math for the excitatory subsystem here. The inhibitory center manifold M_i must be solved for numerically.

The excitatory manifold is solvable with the ansatz $e_2 = e_1 = M_e(e_1)$. Plugging this in gives us,

$$\frac{dM_e}{de_1} = \frac{-e_1+f(b+g_{ee}e_1)}{-e_1+f(b+g_{ee}e_1)} = 1 \quad \text{(Equation 24)}$$

$\frac{dM_e}{de_1} = 1$ can be solved very easily by separation of variables, giving us $M_e(e_1) = e_1$, thereby proving that the ansatz is valid.

Continuing onward, we have the dynamics constrained on a one-dimensional manifold $e := M_e$ and $M(i) := M_i$. Here, we have switched to e and $M(i)$ to emphasize the fact that i is no longer in the same coordinates as i_1 and i_2.

$$\tau\frac{de}{dt} = -e+f(b+g_{ee}e) \quad \text{(Equation 25)}$$

$$\tau\frac{di}{dt} = -i+f(b-g_{ii}M(i)) \quad \text{(Equation 26)}$$

We can now expand this using a Taylor series.

$$\begin{aligned}\tau\frac{de}{dt} &= -e^*+f(b+g_{ee}e^*)+(e-e^*)(g_{ee}f'(b+g_{ee}e^*)-1)\\ &+\frac{g_{ee}^2}{2}(e-e^*)^2f''(b+g_{ee}e^*)+\frac{g_{ee}^3}{6}(e-e^*)^3f^{(3)}(b+g_{ee}e^*)+O(e^4)\end{aligned} \quad \text{(Equation 27)}$$

$$\begin{aligned}\tau\frac{di}{dt} &= -i^*+f(b-g_{ii}M(i^*))+(i-i^*)[-g_{ii}M'(i^*)f'(b-g_{ii}M(i^*))-1]\\ &+\frac{g_{ii}^2(i-i^*)^2}{2}\left[M'(i^*)^2f''(b-g_{ii}M(i^*))+M''(i^*)f'(b-g_{ii}M(i^*))\right]\\ &-\frac{g_{ii}^3i(i-i^*)^3}{6}\left[M'(i^*)^3f^{(3)}(b-g_{ii}M(i^*))+3M'(i^*)M''(i^*)f''(b-g_{ii}M(i^*))+M^{(3)}(i^*)f'(b-g_{ii}M(i^*))\right]\\ &+O(i^4)\end{aligned}$$

Using a change of variables, we can convert the above equations into two depressed cubics giving us

$$\tau\frac{d\hat{e}}{dt} = k_e+a_e\hat{e}-\hat{e}^3$$

$$\tau\frac{d\hat{i}}{dt} = k_i+a_i\hat{i}-\hat{i}^3$$

where

$$\hat{e} = e-\frac{f''}{\left(g_{ee}f^{(3)}\right)} \quad \text{(Equation 28)}$$

$$k_e = \frac{8\left(\frac{3}{4}(f)\left(f^{(3)}\right)^2+\frac{1}{40}(f'')^3 - \frac{27}{50}\left(f' - \frac{1}{g_{ee}}\right)(f'')\right)}{g_{ee}^3\left(f^{(3)}\right)^3}$$

$$a_e = \frac{\frac{1}{6}\left(f^{(3)}\right)\left(f' - \frac{1}{g_{ee}}\right) - \frac{1}{4}(f'')^2}{3\left(g_{ee}^2 f^{(3)}\right)^2}$$

$$\begin{aligned}
\widehat{i} &= i - \frac{1}{g_{ii}}\frac{M'(i^*)^2 f''(b - g_{ii}M(i^*)) - M''(i^*)f'(b - g_{ii}M(i^*))}{-M'(i^*)^3 f^{(3)}(b - g_{ii}M(i^*))+3M'(i^*)M''(i^*)f''(b - g_{ii}M(i^*)) - M^{(3)}(i^*)f'(b - g_{ii}M(i^*))}\\
a_i &= \frac{1}{g_{ii}^2}A_i\alpha_i\\
\alpha_i &= \frac{(-M'(i^*)f'(b - g_{ii}M(i^*)) - 1)}{18f(b - g_{ii}M(i^*))^2}\\
A_i &= \left(-M'(i^*)^3 f^{(3)}(b - g_{ii}M(i^*)) + 3M'(i^*)M''(i^*)f''(b - g_{ii}M(i^*))\right.\\
&\quad \left. - M^{(3)}(i^*)f'(b - g_{ii}M(i^*)) - \frac{1}{4}\left(M'(i^*)^2 f''(b - g_{ii}M(i^*)) - M''(i^*)f'(b - g_{ii}M(i^*))\right)^2\right.\\
k_i &= \frac{N_i}{g_{ii}^3 d_i}\\
N_i &= 8\frac{1}{40}\left(M'(i^*)^2 f''(b - g_{ii}M(i^*)) - M''(i^*)f'(b - g_{ii}M(i^*))\right)^3\\
&\quad -\frac{27}{50}\left(-M'(i^*)f'(b - g_{ii}M(i^*)) - \frac{1}{g_{ii}}\right)\left(M'(i^*)^2 f''(b - g_{ii}M(i^*)) - M''(i^*)f'(b - g_{ii}M(i^*))\right)\\
&\quad +\frac{3}{4}f(b - g_{ii}M(i^*))\left(-M'(i^*)^3 f^{(3)}(b - g_{ii}M(i^*))+3M'(i^*)M''(i^*)f''(b - g_{ii}M(i^*)) - M^{(3)}(i^*)f'(b - g_{ii}M(i^*))\right)^2\\
d_i &= \left(-M'(i^*)^3 f^{(3)}(b - g_{ii}M(i^*))+3M'(i^*)M''(i^*)f''(b - g_{ii}M(i^*)) - M^{(3)}(i^*)f'(b - g_{ii}M(i^*))\right)^2
\end{aligned}$$

(Equation 29)

Whenever k_e, and a_e, or k_i, and a_i are 0, then the two systems undergo a cusp bifurcation. While the exact values of the cusp bifurcation is complicated, especially in the case of the inhibitory system, it still can undergo the bifurcation.

Coupling mutual excitation with inhibition

Now that we have calculated the normal form for both subsystems, we can couple them together. We don't need to explicitly use the normal form at first. Rather its mere existence will be used later. We begin by introducing the coupling terms ϵ. The corresponding equation becomes

$$\tau\frac{de_1}{dt} = -e_1 + f(b + g_{ee}e_2 - \varepsilon[g_{ie}\theta_{i11}i_1 + g_{ie}\theta_{i12}i_2]) \quad \text{(Equation 30)}$$

$$\tau\frac{de_2}{dt} = -e_2 + f(b + g_{ee}e_1 - \epsilon[g_{ie}\theta_{i21}i_1 + g_{ie}\theta_{i22}i_2]) \quad \text{(Equation 31)}$$

$$\tau\frac{di_1}{dt} = -i_1 + f(b - g_{ii}i_2 + \epsilon[g_{ei}\theta_{e11}e_1 + g_{ei}\theta_{e12}e_2]) \quad \text{(Equation 32)}$$

$$\tau\frac{di_2}{dt} = -i_2 + f(b - g_{ii}i_1 + \epsilon[g_{ei}\theta_{e21}e_1 + g_{ei}\theta_{e22}e_2]) \quad \text{(Equation 33)}$$

Here, $\theta_{k1}^2 + \theta_{k2}^2 = 1$ and $\theta_{kx} > 0$. This allows the coupling between the connections to be arbitrary. We can think of θ as a way to parameterize the asymmetries in synaptic weights between the coupling.

Next, by expanding the function f as a Taylor series with respect to ϵ centered at $\epsilon = 0$, and then disregarding order ϵ^2 and above, we get

$$\tau\frac{de_1}{dt} = -e_1 + f(b_e + g_{ee}e_2) - \epsilon f'(b_e + g_{ee}e_2)(g_{ie}\theta_{i11}i_1 + g_{ie}\theta_{i12}i_2) \quad \text{(Equation 34)}$$

$$\tau\frac{de_2}{dt} = -e_2 + f(b_e + g_{ee}e_1) - \epsilon f'(b_e + g_{ee}e_1)(g_{ie}\theta_{i21}i_1 + g_{ie}\theta_{i22}i_2) \quad \text{(Equation 35)}$$

$$\tau\frac{di_1}{dt} = -i_1 + f(b_i - g_{ii}i_2) + \epsilon f'(b_i - g_{ii}i_2)(g_{ei}\theta_{e11}e_1 + g_{ei}\theta_{e12}e_2) \quad \text{(Equation 36)}$$

$$\tau\frac{di_2}{dt} = -i_2 + f(b_i - g_{ii}i_1) + \epsilon f'(b_i - g_{ii}i_1)(g_{ei}\theta_{e21}e_1 + g_{ei}\theta_{e22}e_2) \quad \text{(Equation 37)}$$

We can then make the substitution for the stable attractive manifolds we made above such that $e = e_2 = M(e_1) = e_1$ and $i = i_2 = M_i(i_1)$.

$$\tau\frac{de}{dt} = -e + f(b_e + g_{ee}e) - \epsilon f'(b_e + g_{ee}e)(g_{ie}(\theta_{i11} + \theta_{i21})i + g_{ie}(\theta_{i12} + \theta_{i22})M_i(i)) \quad \text{(Equation 38)}$$

$$\tau\frac{di}{dt} = -i + f(b_i - g_{ii}M_i(i)) + \epsilon f'(b_i - g_{ii}M_i(i))(g_{ei}(\theta_{e11} + \theta_{e21})e + g_{ei}(\theta_{e12} + \theta_{e22})e) \quad \text{(Equation 39)}$$

For ease of notation let $\theta_{i_1} = \theta_{i11} + \theta_{i21}$ and $\theta_{i_2} = \theta_{i12} + \theta_{i22}$, and $\theta_{e_1} = \theta_{e11} + \theta_{e21}$ and $\theta_{e_2} = \theta_{e12} + \theta_{e22}$ We can now expand the equation in terms of e and i giving us

$$\begin{aligned}\tau\frac{de}{dt} &= -e^* + f(b + g_{ee}e^*) + (g_{ee}f'(b + g_{ee}e^*) - 1) + \frac{g_{ee}^2(e - e^*)^2}{2}f''(b + g_{ee}e^*) \\ &+ \frac{g_{ee}^3(e - e^*)^3}{6}f^{(3)}(b + g_{ee}e^*) + O(e^4) - \epsilon f'(b_e + g_{ee}e)\left(g_{ie}\theta_{i1} + g_{ie}\theta_{i_2}M_i'(i)\right)(i - i^*) + O(i^2)\end{aligned} \quad \text{(Equation 40)}$$

$$\begin{aligned}\tau\frac{di}{dt} &= -i^* + f(b - g_{ii}M(i^*)) + (i - i^*)[\\ &- g_{ii}M'(i^*)f'(b - g_{ii}M(i^*)) - 1] + \frac{g_{ii}^2(i - i^*)^2}{2}\left[M'(i^*)^2f''(b - g_{ii}M(i^*)) + M''(i^*)f'(b - g_{ii}M(i^*))\right]\end{aligned} \quad \text{(Equation 41)}$$

$$-\frac{g_{ii}^3(i - i^*)^3}{6}\left[M'(i^*)^3f^{(3)}(b - g_{ii}M(i^*)) + 3M'(i^*)M''(i^*)f''(b - g_{ii}M(i^*)) + M^{(3)}(i^*)f'(b - g_{ii}M(i^*))\right] \quad \text{(Equation 42)}$$

$$+ O(i^4) + \epsilon f'(b_i - g_{ii}M_i(i))\left(g_{ei}\theta_{e1} + g_{ei}\theta_{e_2}\right)(e - e^*) + O(e^2) \quad \text{(Equation 43)}$$

Recall we can create a depressed cubic in the uncoupled system using Equations 28 and 29 to get

$$\tau\frac{dE}{dt} = k_e(b, g_e e) - a_e(b, g_e e)E - E^3 - \left(\epsilon f'(b_e + g_{ee}e^*)\left(g_{ie}\theta_{i1} + g_{ie}\theta_{i_2}M_i'(i^*)\right)\right)(I + I^*) \quad \text{(Equation 44)}$$

$$\tau\frac{dI}{dt} = k_i(b, g_e e) - a_i(b, g_e e)I - I^3 + \epsilon f'(b_i - g_{ii}M_i(i^*))\left(g_{ei}\theta_{e1} + g_{ei}\theta_{e_2}\right)\left(E + \frac{f''}{\left(g_{ee}f^{(3)}\right)}\right) \quad \text{(Equation 45)}$$

where $I^* = \frac{1}{g_{ii}}\frac{M'(i^*)^2f''(b - g_{ii}M(i^*)) - M''(i^*)f'(b - g_{ii}M(i^*))}{-M'(i^*)^3f^{(3)}(b - g_{ii}M(i^*)) + 3M'(i^*)M''(i^*)f''(b - g_{ii}M(i^*)) - M^{(3)}(i^*)f'(b - g_{ii}M(i^*))}$ from Equation 29. To clean everything up a bit, we can recast our equations as

$$\tau\frac{dE}{dt} = k_e^* - a_eE + E^3 - \epsilon a_{ie}I \quad \text{(Equation 46)}$$

$$\tau\frac{dI}{dt} = k_i^* - a_iI - I^3 - \epsilon a_{ei}E \quad \text{(Equation 47)}$$

where $a_{ie} = g_{ie}\theta_{i1} + g_{ie}\theta_{i2}M'$, $a_{ei} = g_{ei}\theta_{e1} + g_{ei}\theta_{e2}$, $k_e^* = k_e + \frac{f''}{(g_{ee}f^{(3)})}$, and $k_i^* = k_i + I^*$.

QUANTIFICATION AND STATISTICAL ANALYSIS

Equilibrium points in microcircuits

It is conceivable that the functional repertoire of a motif is correlated to the abundance of its dynamical states. Here, we employ a statistical approach that provides us an estimate of the number of equilibrium points in the relevant parameter space. We compared motifs that are specifically chosen to highlight the presence or absence of recurrent loops, along with some randomly chosen feed-forward motifs (Figure 1B). After sweeping through the parameter space, we then estimated the number of equilibrium points in each trial by counting the number of clusters (Figure S1A).

Parameter space

For a four neuron motif, there are 12 possible synaptic connections. To lower dimensionality in parameters, we constrained synaptic weights with the same type of pre-synaptic and post-synaptic neuron to have the same value, except for threshold-based filtering (Figure 1A). Thus, we have four types of synaptic weights: excitatory-to-excitatory (g_{ee}), excitatory-to-inhibitory (g_{ei}), inhibitory-to-inhibitory (g_{ii}) and inhibitory-to-excitatory (g_{ie}). For each motif, we ran simulations over 18900 trials, where each trial has a different synaptic weight parameter set g_{ee}, g_{ie}, g_{ii} (Table S1).

Aside from synaptic weights, we also iterated through different underlying bias currents in the neurons. The bias currents adjust the threshold for firing, allowing inhibitory neurons to fire in the absence of excitatory input (Table S1). This ensures that we capture the dynamic states produced by the inhibitory neurons. For each trial, a brief injected current goes into different pairs of neurons, for example one trial would stimulate E_1 only, and another would stimulate E_1 and I_1 simultaneously. This is run through all possible pairs. The amplitude of the stimulus changes as well. Both stimulating different pairs and varying the stimulus amplitude ensure a wider exploration of the parameter space, thereby allowing us to find more equilibrium points. Each brief pulse of positive stimulation is separated by a negative reset signal. These are shown in Figure S1B. Note that this method may not capture every single equilibrium point present, nor will it be able to detect other stable structures such as limit cycles. Nevertheless, the parameter sweeping still provides valuable information regarding the complexity of the dynamical states of the system.

Clustering

To analyze the amount of equilibrium points present in each trial, we look at the firing rate trace of the motif across the four-dimension space (e_1, e_2, i_1, i_2). The firing rate is calculated using a sliding window of 50 ms over spikes, and sampled at an interval of 10 ms. We used the elbow method to obtain the number of clusters in the firing rate trace of the trial.[71] The elbow method detects the number of clusters by iterating through the possible number of clusters k and performing K-means clustering, and then evaluating each guess k with its standard deviation, which is $SSE = \sum_{i=1}^{k} \sqrt{\frac{\sum_{j=1}^{N_i} (r_{ij} - \bar{r}_i)^2}{N_i - 1}}$. By plotting SSE as a function of k, we see that sometimes the plot has a sharp drop in SSE followed by a shallow decrease when k becomes large. The sharp drop is cleverly termed "the elbow" (Figure S1A). Such a sharp drop usually indicates that the number of clusters assigned has hit the correct amount. If no elbows are present, then the data set most likely only has one cluster. A criterion is needed to determine "how sharp" a drop can be considered an elbow, and these criteria is set so that the slope of the "arm" must be seven times the slope of the "forearm".

We purposely neglected the transient activities 100ms after a positive stimulation pulse or a negative reset signal in order to neglect "fake" clusters (i.e. clusters that are present, but are not true equilibrium points). Finally, the total number of equilibrium points in all possible parameter sets, which total up to 18900 trials, are calculated for each motif for comparison.

CPG in microcircuits

Another important computation for small motifs is the ability to generate oscillations under constant input. Similar to how the equilibrium points were counted, for CPGs, the parameter space was scanned across suitable values of g_{ie} and g_{ei}. For each trial, we then determine whether the motif under said parameter set was capable of oscillation. The ISI for each trial was calculated, and rounded to the nearest 0.001 (s). Since there is no noise in the system, the periodic firing of a neuron being driven by a constant current has a near perfect period (where the slight differences were accounted for by the rounding procedure), and thus the ISI would consist of one single value. The choice of rounding, 0.001 (s), is hence chosen so that when receiving a constant bias current with no noise, the ISI will be 1 single value, as it should be. For any rounding numbers smaller than that, for example 0.0005 (s), such trials will yield 2 or more ISI values, which is due to the time step choices of the simulator and does not really reflect whether the motif is in a CPG mode. For CPGs, the ISI would contain two or more values. The counts for trials with CPGs were calculated for each motif.

Decision-making and bistability

To further illustrate how feedback and mutual inhibition differ in terms of functions, we focused on two functions in particular: decision-making and bistability. We swept through the relevant parameter space, and observed whether motifs with or without mutual inhibition could perform these two functions. Once again, to lower the dimensionality of the parameter space, we constrained

synaptic weights with the same type of pre-synaptic and post-synaptic neuron to have the same value. For bistability, since it happens within the excitatory subsystem, the most crucial synaptic weight is g_{ee}. For decision-making in feedback inhibitory networks, the important synaptic weight is g_{ie}, since strong g_{ie} allows the circuit to turn off the unfavorable excitatory neuron. For decision-making in mutual inhibitory networks, the key synaptic weight is g_{ii}. Therefore, for the purpose of this analysis, we will hold g_{ei} constant and sweep through relevant parameter regimes of g_{ee}, g_{ie} and g_{ii}. The parameters are listed in Table S2.

For each point (g_{ee}, g_{ie}, g_{ii}) in the parameter space, two trials with different input protocols are given to the network. The bistable protocol gives a 100 ms positive pulse to one of the excitatory neurons, resets the circuit using a strong negative pulse, and repeats this process for all of the excitatory neurons present within the network (Figure S2). If the network is capable of bistability, then the pulse to one of the excitatory neurons should be able to turn the network to the ON state and remain there until the resetting pulse comes in. Therefore, if the circuit stays on after E_1 is excited, and also stays on after E_2 is excited, then it is classified as being able to perform the switch function.

The decision protocol iterates through all possible pairs of excitatory neurons, where for each time period, each pair is given an asymmetrical input (Table S2). If the network decides, then there will be a difference in firing rate between a pair of neurons at that time period. The condition for deciding is that the "winning" neuron (if one neuron's time-averaged firing rate is 10 Hz larger than the other, it is considered a winner) must switch as the relative input strength switches. For instance, if E_1 wins when input 1 is larger than input 2, then E_2 must win when input 2 is larger than input 1. For motif B, decision is made between the excitatory neurons, hence the aforementioned analysis is performed on the two excitatory neurons. The decision is made between the inhibitory neurons for motif A, hence the decision analysis here is performed on I_1 and I_2. Each point (g_{ee}, g_{ie}, g_{ii}) will be capable of either bistability, quasi-decision, decision, both, or none. The results are then drawn into a heat map, where broader regions of "both functions present" mean that it is more possible for the two functions to co-exist.

Entropy

For a discrete random variable X, where there are n potential outcomes $x_i, \ldots x_n$ with associated probability $P(x_1), \ldots P(x_n)$, its entropy is

$$H(X) = -\Sigma_{i=1}^{n} P(x_i) \log P(x_i) \quad \text{(Equation 48)}$$

Entropy of words, H_{word}

After the pulse is turned off and before the reset signal arrives, each neuron i will have a different time-averaged firing rate $\overline{r_i} = \langle r_i \rangle_t$, which represents the "state" the neuron is in for that particular equilibrium point. Together, these firing rates can form a sequence, i.e. $r_1, r_2, r_3, \ldots r_{100}$, which we call a "word". Each trial will produce one such word. If the memory network has multiple equilibrium points, then the variation of words would be large, and the entropy resulting from such a distribution of words, H_{word}, would be large.

When calculating the entropy, what we actually used is the quotient of $\overline{r_i}$ over 20. This is similar to grouping the firing rate into different bins, where the firing rates within the same bin are assumed to carry the same amount of information. The choice of having a 20 Hz bin is arbitrary – qualitatively similar results can be obtained by other bins, such as 30 Hz and 40 Hz as well.

Entropy of symbols, H_{symbol}

A word $r_1, r_2, r_3, \ldots r_{100}$ itself is a distribution of firing rates. The entropy of this distribution is called H_{symbol}, which reflects how widely distributed these firing rates are. For the word produced by each trial, its entropy of symbols is calculated, and then averaged across trials.

Entropy of binary symbols, H_{binary}

Instead of representing each neuron by its firing rate, we instead observe whether the neuron fires or not. If it fires, the neuron is given a label $I_i = 1$, and $I_i = 0$ otherwise. This again forms a distribution across the neuron population, $I_1, I_2, I_3, \ldots I_{100}$, and its associated entropy is called H_{binary}.